Journal of the Geological Society, London, Vol. **171**, 2014, pp. 465–479. http://dx.doi.org/10.1144/jgs2013-115
Published *Online First* on May 28, 2014

Behaviour of zircon and monazite during crustal melting

CHRIS YAKYMCHUK* & MICHAEL BROWN
Laboratory for Crustal Petrology, Department of Geology, University of Maryland, College Park, MD 20742-4211, USA
**Corresponding author (e-mail: cyak@umd.edu)*

Abstract: Ages retrieved from accessory minerals in high-grade metamorphic rocks place important constraints on the timing of events and the rates of tectonometamorphic processes operating in the deep crust. In suprasolidus rocks, the dissolution and growth of zircon and monazite are strongly dependent on the *P–T* conditions of metamorphism and the chemistry and quantity of anatectic melt present. Along a clockwise *P–T* path, prograde heating above the solidus leads to episodic melt loss and changes in melt chemistry that have important implications for the dissolution and growth of zircon and monazite. In this study, phase equilibria modelling of open-system melting is coupled with experimental data on zircon and monazite solubility to evaluate the stability of these minerals at suprasolidus conditions along several schematic clockwise *P–T* paths. In migmatite melanosomes and residual granulites, some zircon is expected to survive heating to peak temperature and subsequent isothermal decompression, whereas monazite may be completely consumed, consistent with the observation that inherited cores are less common in monazite than in zircon. After decompression, during cooling to the solidus, new zircon and monazite growth from melt trapped along grain boundaries in melanosomes and residual granulites is expected to be limited. By contrast, leucosomes in migmatites and anatectic granites are predicted to contain mostly newly formed zircon and monazite with minimal inherited components, unless significant entrainment of these minerals from the source occurs. The preservation of cores inside newly formed zircon, as observed in many anatectic granites, demonstrates that segregation, ascent and emplacement is commonly fast enough to limit dissolution of these inherited grains.

Accessory minerals such as zircon and monazite are important in studies of high-grade migmatites and residual granulites, and related anatectic granites, because they may be dated using isotopic or chemical methods. Thus, these minerals have the potential to place temporal constraints on metamorphic *P–T* paths retrieved from migmatites and residual granulites, especially if accessory mineral growth can be tied to a particular part of the *P–T* path (Rubatto 2002; Harley *et al.* 2007; Williams *et al.* 2007; Kelsey *et al.* 2008; Reno *et al.* 2012; Korhonen *et al.* 2013*a*), and to provide crystallization ages for anatectic granites. For example, sometimes it is possible to link ages obtained from accessory minerals to specific metamorphic reactions or to particular coexisting minerals (Degeling *et al.* 2001; Hermann & Rubatto 2003; Whitehouse & Platt 2003; Rubatto *et al.* 2006, 2013; Harley & Kelly 2007; Harley *et al.* 2007; Baldwin & Brown 2008), which may allow constraints to be placed on rates of orogenic processes as well as the timing of events. However, our knowledge of the dissolution and growth of zircon and monazite in suprasolidus crust in relation to the *P–T* evolution and the changing bulk chemistry during melting is limited to a few pioneering studies (Kelsey *et al.* 2008; Spear & Pyle 2010; Kelsey & Powell 2011; Skrzypek *et al.* 2012). In particular, the role of open-system melting and melt loss on the stability of accessory minerals in suprasolidus rocks has received insufficient attention given that the ages obtained from these minerals are integral to documenting the nature and time scales of tectonometamorphic processes in the residual deep crust.

Partial melting of the deep crust and drainage of melt to the shallow crust is the principal mechanism by which the continental crust is chemically differentiated into a refractory lower portion and a complementary enriched upper portion. At the local scale, suprasolidus crust may behave as a closed (melt is retained) or open (melt is drained) or conditionally open (cyclic closed and open) system (Handy *et al.* 2001; Brown 2013). Melt extraction in conditionally open systems is expected to occur when the melt connectivity transition is reached at *c.* 7 vol% melt (Rosenberg & Handy 2005). Relatively fertile clastic metasedimentary rocks may produce up to 50–60 vol% melt at 900 °C in granulite and ultrahigh-temperature (UHT) metamorphic terranes (Clemens 2006). Therefore, such rocks are expected to experience multiple melt loss events during a single orogenic cycle (Brown 2013). As melt is drained from the source, the bulk composition becomes progressively more residual and the chemistry of the melt in equilibrium with the residue evolves accordingly.

The behaviour of zircon and monazite under suprasolidus conditions is complex, being controlled by both physical and chemical factors (Brown 2013). These factors include the following: the microstructural location of the accessory minerals, whether they occur along grain boundaries or sequestered as inclusions, and the stability of the major rock-forming minerals if they occur as inclusions (Watson *et al.* 1989; Bea *et al.* 2006); the kinetics of dissolution (Bea 1996; Watson 1996); the extent of anatexis (Rubatto *et al.* 2001); the chemistry of the melt (Watson & Harrison 1983; Rapp *et al.* 1987; Stepanov *et al.* 2012); the *P–T* path (Roberts & Finger 1997); and the rate of melt extraction (Watt *et al.* 1996). A further complication is the crystal-size distribution and the role that Ostwald ripening might play during the prograde evolution (Nemchin & Bodorkos 2000; Nemchin *et al.* 2001). In this study, phase equilibria modelling of pelite and greywacke along four schematic *P–T* paths is coupled with experimental data for zircon and monazite solubility to evaluate the consequences of melt loss on the dissolution and growth of zircon and monazite in residual source rocks, extending the discussion begun by Kelsey *et al.* (2008).

Methods

Phase equilibria modelling

The *P–T* conditions at which fluid-absent melting occurs and the quantity and the chemistry of melt produced from clastic metasedimentary rocks during closed-system melting may be determined by

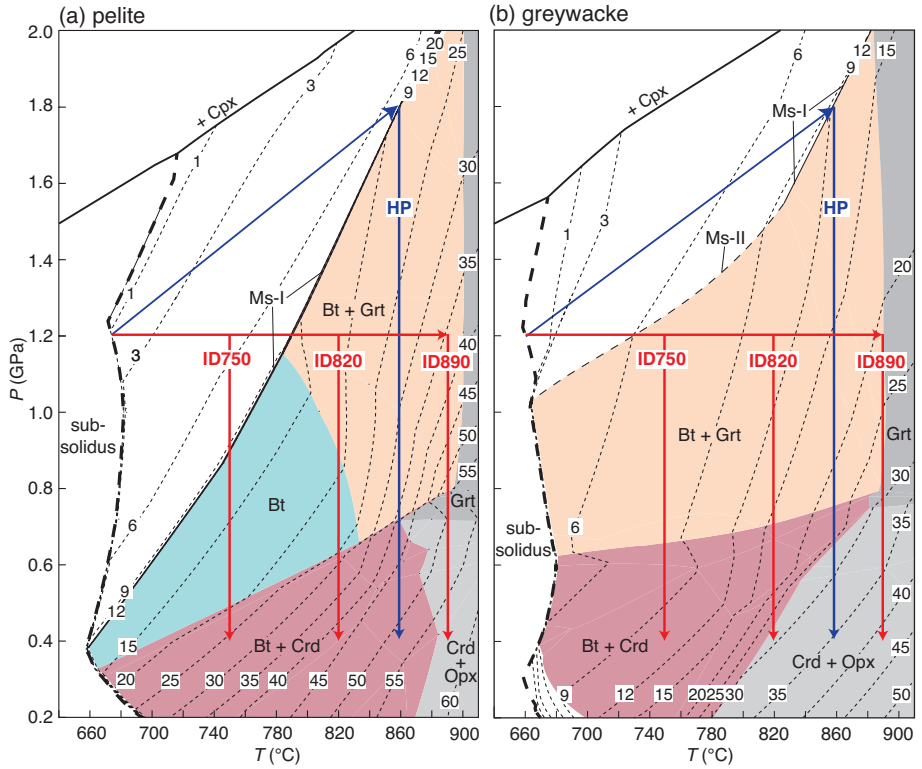

Fig. 1. Simplified pressure–temperature (*P–T*) phase diagrams calculated for closed-system melting for (**a**) an average amphibolite-facies pelite, and (**b**) an average passive margin greywacke (modified from Yakymchuk & Brown 2014). Bt, biotite; Cpx, clinopyroxene; Crd, cordierite; Grt, garnet; Ms, muscovite; Opx, orthopyroxene. Shaded fields are the principal stability fields of the major rock-forming ferromagnesian minerals. Lines 'Ms–I' and 'Ms–II' represent the boundaries for the muscovite to K-feldspar reaction and the K-feldspar-absent muscovite-out reaction, respectively. The bold dashed line is the fluid-present solidus and the short dashed lines represent isopleths of mol% melt (approximately equivalent to vol% melt in nature). Four schematic *P–T* paths are shown. These diagrams are derived from the fully labelled pseudosections presented by Yakymchuk & Brown (2014). Most melt mol% isopleths have positive slopes, which indicates that melt is produced during heating and decompression.

forward modelling using *P–T* pseudosections constructed for the initial bulk chemical compositions (e.g. White *et al.* 2007; Johnson *et al.* 2008; Brown & Korhonen 2009). In addition, by using a series of *P–T* pseudosections calculated for bulk chemical compositions modified by a succession of melt loss events, the effects of melt loss on future melt production, total melt production, and melt chemistry on the preservation of peritectic mineral assemblages may be evaluated for open-system behaviour (White & Powell 2002; Brown & Korhonen 2009; Korhonen *et al.* 2010*a*; Yakymchuk & Brown 2014).

In this study, calculations were performed using THERMOCALC v.3.35 (Powell & Holland 1988) and the internally consistent dataset of Holland & Powell (1998) together with the most recent activity–composition (*a–x*) models for the phases of interest, which have been listed by Yakymchuk & Brown (2014). Modelling was undertaken in the Na_2O–CaO–K_2O–FeO–MgO–Al_2O_3–SiO_2–H_2O–TiO_2–Fe_2O_3 chemical system, which is currently the most realistic system to investigate melting for clastic metasedimentary rocks (White *et al.* 2007). Two rock types were considered: an average amphibolite-facies pelite (Ague 1991) and an average passive margin greywacke (Yakymchuk & Brown 2014). The amount of water in the modelled compositions for the pelite and the greywacke was adjusted so that there is minimal (<0.1 mol%) free H_2O at the solidus at 1.2 GPa, which is consistent with fluid-absent conditions above the solidus (White & Powell 2002; White *et al.* 2003, 2005). If the modelled prograde path crossed the solidus at lower or higher pressures, the quantity of melt produced will be slightly overestimated and underestimated, respectively. The chemistry and quantity of melt expected at *P–T* was determined using the 'read rbi' script in THERMOCALC.

In this study, the range of pressures and temperatures modelled is typical of those retrieved from migmatites and high-pressure granulites in orogenic belts (e.g. Harley 1998; Teyssier & Whitney 2002; O'Brien & Rötzler 2003). After prograde heating to the metamorphic peak, near-isothermal decompression is commonly documented in migmatite–gneiss domes (Whitney *et al.* 2013) and in granulites (Harley 1998), consistent with clockwise *P–T* paths. Furthermore, many granulites and ultrahigh-temperature metamorphic rocks record close to isobaric cooling after decompression (Harley 1998).

Crustal melting is modelled for each of the two rock types along four schematic clockwise *P–T* paths as shown in Figure 1, which is a closed-system *P–T* phase diagram simplified from the *P–T* pseudosections of Yakymchuk & Brown (2014). However, during orogenesis melt drainage from the anatectic zone to shallow crustal levels is to be expected (Brown 2013). Thus, this study concentrates on open-system crustal melting. Open-system melting for the same four *P–T* paths is modelled as follows. At each point along the *P–T* path where the melt fraction reaches the melt connectivity transition of 7 mol% (*c.* 7 vol% in nature), six-sevenths of the melt produced is removed from the bulk chemical composition, leaving one-seventh (*c.* 1 vol% in nature) that is assumed to have been retained on grain boundaries (Yakymchuk & Brown 2014). After a melt loss event, the residual bulk chemical composition is used to calculate a new *P–T* pseudosection that remains valid until the next melt loss event is reached. Figures 2 and 3 are *P–T* phase diagrams for open-system melting simplified from the pseudosections of Yakymchuk & Brown (2014); that study also includes a discussion of the general effects of melt loss on melt production and tectonics.

Three of the four *P–T* paths modelled for open-system behaviour comprise three segments: an isobaric heating segment at 1.2 GPa beginning at the solidus and extending to the peak temperature, an isothermal decompression segment from 1.2 to 0.7 or 0.4 GPa at three different peak temperatures (750, 820 and 890 °C), and an isobaric cooling segment starting at 0.7 or 0.4 GPa and extending to the solidus (Fig. 2). These peak temperatures were chosen so that the *P–T* paths cross the main hydrate-breakdown melting reactions typically encountered by pelites and greywackes during exhumation after collisional orogenesis (see Yakymchuk &

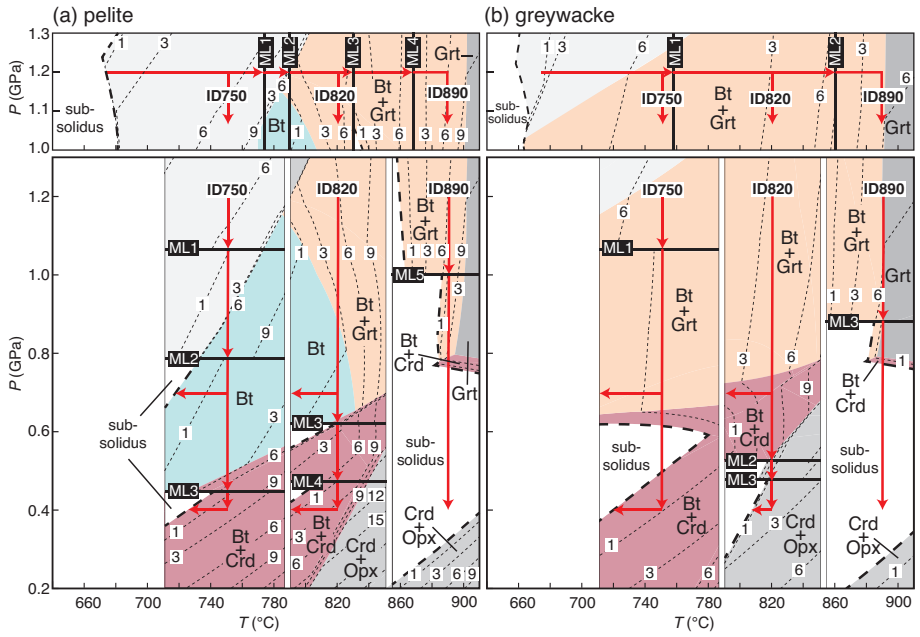

Fig. 2. Composite *P–T* diagrams for conditionally open-system melting for each of the isobaric heating–isothermal decompression *P–T* paths (paths ID750, ID820 and ID890 in Fig. 1) modelled for (**a**) pelite and (**b**) greywacke. Also labelled are isobaric cooling paths at 0.7 and 0.4 GPa from the decompression segment of the *P–T* path to the solidus for paths ID750 and ID820. Each diagram comprises a series of panels that are arranged from low to high temperature and stacked from high to low pressure calculated for incrementally melt-depleted bulk compositions along each *P–T* path. The bold dashed line is the fluid-absent solidus and the fine dashed lines represent isopleths of mol% melt (approximately equivalent to vol% melt in nature). Each panel shows melt mol% isopleths and the stability field of major ferromagnesian minerals. Melt loss (ML) events are located on the seams between the panels. After a melt loss event, the solidus is displaced to higher temperatures and melt isopleths generally become steeper at pressures above the stability field of cordierite. Therefore, the amount of melt produced during decompression in a conditionally open system is less than that for a closed system (Fig. 1).

Brown 2014). The fourth *P–T* path modelled is a clockwise *P–T* path that reaches peak high-pressure granulite-facies conditions of 1.8 GPa at 860 °C after prograde heating from the solidus at 1.2 GPa and before isothermal decompression and isobaric cooling to the solidus at 0.7 or 0.4 GPa (Fig. 3).

Zr and LREE concentrations of the source and melt

The amount of zircon and monazite dissolution during crustal melting is dependent on the bulk-rock concentrations of zirconium (Zr) and light rare earth elements (LREE) in the source, and the concentration of these elements required to saturate the anatectic melt assuming that the melt does not drain from the system prior to saturation. The solubility of zircon and monazite varies with *P–T* and the major element chemistry of the melt. In this study, the major element chemistry of the melt along each *P–T* path is retrieved from THERMOCALC and combined with solubility equations for zircon and monazite.

For zircon, we use the solubility equation of Boehnke *et al.* (2013). Using the zircon solubility equation of Kelsey *et al.* (2008), which is based on the experimental data of Harrison & Watson (1983), produces an indistinguishable difference in the zircon dissolution plots discussed below. For monazite there are two alternative solubility equations that yield different rates of dissolution. Kelsey *et al.* (2008) presented a solubility equation for monazite based on the experimental data of Rapp *et al.* (1987). More recently, Stepanov *et al.* (2012) developed a solubility equation for monazite that is more strongly dependent on temperature and the amount of water in the anatectic melt than the equation of Kelsey *et al.* (2008). Based on their new solubility equation, Stepanov *et al.* (2012) argued that unrealistically high LREE concentrations in melt were predicted by the equation of Kelsey *et al.* (2008), and they suggested that the conclusions of Kelsey *et al.* (2008) with respect to differences in the solubility of zircon and monazite require re-evaluation. Therefore, in this study we have used the monazite solubility equations of both Kelsey *et al.* (2008) and Stepanov *et al.* (2012) to calculate the amount of monazite dissolution along the *P–T* paths. This allows for a comparison of both sets of results in relation to evidence from residual migmatites and granulites.

The concentrations of Zr and LREE in pelites and greywackes are broadly similar, with Zr of *c.* 200 ppm and LREE of 150–200 ppm for pelites and Zr of 100–200 ppm and LREE of 50–150 ppm for greywackes (Taylor & McLennan 1985). Metasedimentary migmatites generally have Zr concentrations of 80–270 ppm and LREE concentrations of 30–300 ppm (e.g. Sawyer 1986; Solar & Brown 2001; Guernina & Sawyer 2003; Korhonen *et al.* 2010*b*), although Zr concentrations are >300 ppm in some kinzigites and stronalites of the Ivrea Zone (Bea & Montero 1999). Based on these data, we use initial values of 50, 150 and 300 ppm for both Zr and LREE, which encompass the range of concentrations of most pelites, greywackes and metasedimentary migmatites. In this study, the bulk chemical composition of the system prior to any melt loss is referred to as the protolith composition. After one or more melt loss events the resultant melt-depleted bulk chemical composition is referred to as the source composition.

Zircon and monazite dissolution

The amount of accessory mineral dissolution is calculated following the method of Kelsey *et al.* (2008). First, the saturation concentrations of the melt in ppm are calculated as follows. The major element concentration of the anatectic melt at *P–T* is retrieved from THERMOCALC. This information is combined with (1) the solubility equations of Kelsey *et al.* (2008), Stepanov *et al.* (2012) and Boehnke *et al.* (2013), and (2) stoichiometric concentrations of Zr in zircon (497,664 ppm Zr) and LREE in monazite (566,794 ppm LREE) to determine the saturation concentrations of Zr and LREE

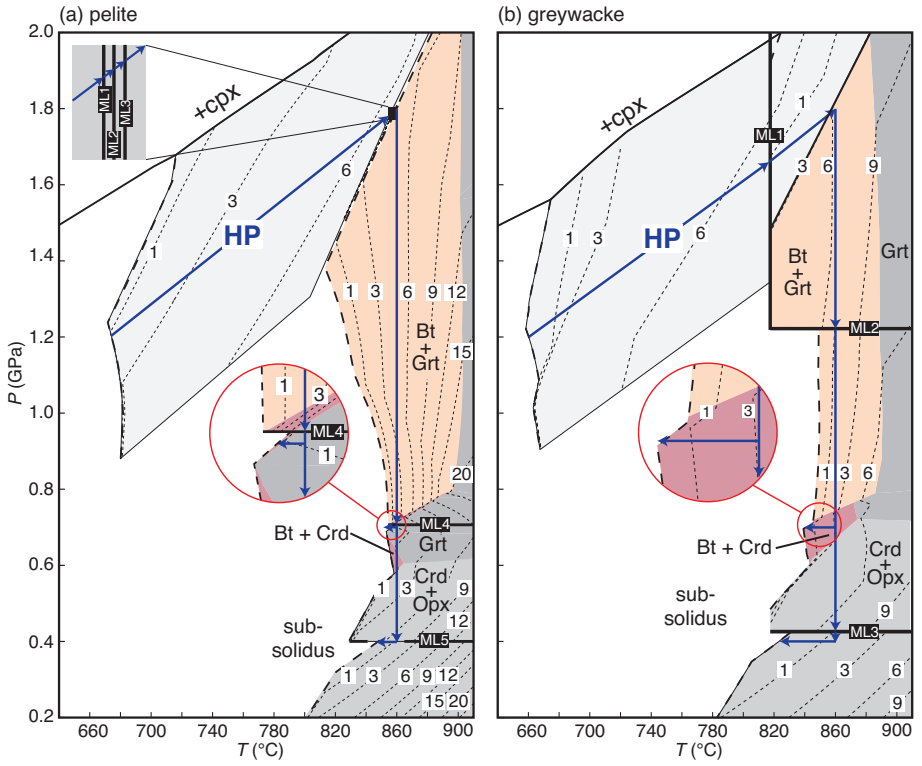

Fig. 3. Composite *P–T* diagrams for conditionally open-system melting for the high-pressure *P–T* path (path HP in Fig. 1) calculated for (**a**) pelite and (**b**) greywacke. Also labelled are isobaric cooling paths at 0.7 and 0.4 GPa from the decompression segment of the *P–T* path to the solidus. Each diagram comprises a series of panels arranged from low to high temperature and stacked from high to low pressure calculated for incrementally melt-depleted bulk compositions. The bold dashed line is the fluid-absent solidus and the fine dashed lines represent isopleths of mol% melt (approximately equivalent to vol% melt in nature). Each panel shows melt mol% isopleths and the stability field of major ferromagnesian minerals. Melt loss (ML) events are located on the seams between the panels. It should be noted that the trajectory of the decompression path is nearly parallel to the melt isopleths for both rock types, which indicates that relatively little melt is produced during decompression. Most melt is generated during heating, although melt is also produced along the low-pressure segment of the decompression path within the stability field of cordierite at $P<0.7$ GPa.

in ppm (Kelsey *et al.* 2008). These 'initial saturation concentrations' do not account for the proportion of anatectic melt nor the bulk-rock concentrations of Zr and LREE.

Second, the initial saturation concentrations of Zr or LREE (ppm) are multiplied by the proportion of anatectic melt (retrieved from THERMOCALC) to arrive at concentrations in ppm that are required to saturate the melt in the equilibration volume of the rock. Finally, these values are divided by the bulk-rock chemical concentrations of Zr and LREE (50, 150 and 300 ppm). The result is the proportion of zircon or monazite dissolution required to saturate the anatectic melt in Zr and LREE in the equilibration volume of the rock. This value is subtracted from 100% and the results are reported as per cent remaining relative to the amount of zircon and monazite existing at the fluid-present solidus for each *P–T* path.

At each melt loss event, the percentage of subsequent zircon and monazite dissolution is normalized to the percentage of zircon and monazite present immediately prior to the melt loss event. Therefore, calculations yield the proportion of zircon or monazite remaining along the *P–T* path relative to the amount of zircon or monazite originally existing at the fluid-present solidus.

Results

Melt production in an undrained (closed) system

Figure 1a and b shows the stability field of major ferromagnesian minerals and the amount of melt produced across the range of *P–T* modelled. For the pelite, the fluid-present solidus is located at 660–680 °C from 0.4 to 1.2 GPa but at higher temperatures at $P<0.4$ GPa and $P>1.2$ GPa. For the greywacke, the fluid-present solidus is located at *c.* 670 °C up to 1.5 GPa. For both the pelite and the greywacke, garnet is stable at high pressures and at high temperatures at $P>0.6$ GPa. Cordierite is stable at $P<0.3$–0.8 GPa with increasing temperature for the pelite (Fig. 1a) and at $P<0.6$–0.7 GPa with increasing temperature for the greywacke (Fig. 1b). Orthopyroxene is stable at $P<0.7$ GPa at $T>840$ °C for the pelite and at $P<0.7$ GPa at temperatures >760 °C for the greywacke. For both rock types, biotite is unstable above 890–900 °C at $P>0.7$ GPa and stable to lower T at $P<0.7$ GPa. The *P–T* field of interest is bounded by the stability of clinopyroxene at high P for both rock types.

The amount of melt present at *P–T* is shown in Figure 1 by melt mol% isopleths. Melt mol% isopleths are generally steep in the stability field of garnet and have shallower slopes in the stability field of cordierite. The melt isopleths for the pelite (Fig. 1a) are more closely spaced than those for the greywacke (Fig. 1b).

For the pelite, the total amount of melt produced along the *P–T* paths ID750, ID820, ID890 and HP is 26, 43, 58 and 52 mol%, respectively (Fig. 1a). For the greywacke, the total amount of melt produced along the *P–T* paths ID750, ID820, ID890 and HP is 11, 29, 42 and 35 mol%, respectively (Fig. 1b). However, as discussed above, this is unrealistic and melt is expected to drain from the system at the melt connectivity transition in nature.

Zircon and monazite behaviour in an undrained (closed) system

For closed-system behaviour, the amount of zircon and monazite dissolution along *P–T* paths ID750, ID820 and ID890 is shown in Figure 4 (redrawn from data of Kelsey *et al.* 2008 for the metapelite and psammite compositions used in their work). In an undrained system, assuming bulk-rock concentrations of 200 ppm Zr and 500 ppm LREE, for the pressure range of interest here (1.2–0.4 GPa), the dissolution contours for zircon and monazite plot with moderate to steep positive slopes in a *P–T* diagram for both the metapelite and psammite.

For an isobaric prograde evolution at 1.2 GPa, zircon persists to ultrahigh temperatures in both the metapelite and the psammite (Fig. 4a and c). Only during decompression along the ID890 path is zircon completely consumed at 0.6 GPa for the metapelite and 0.8 GPa

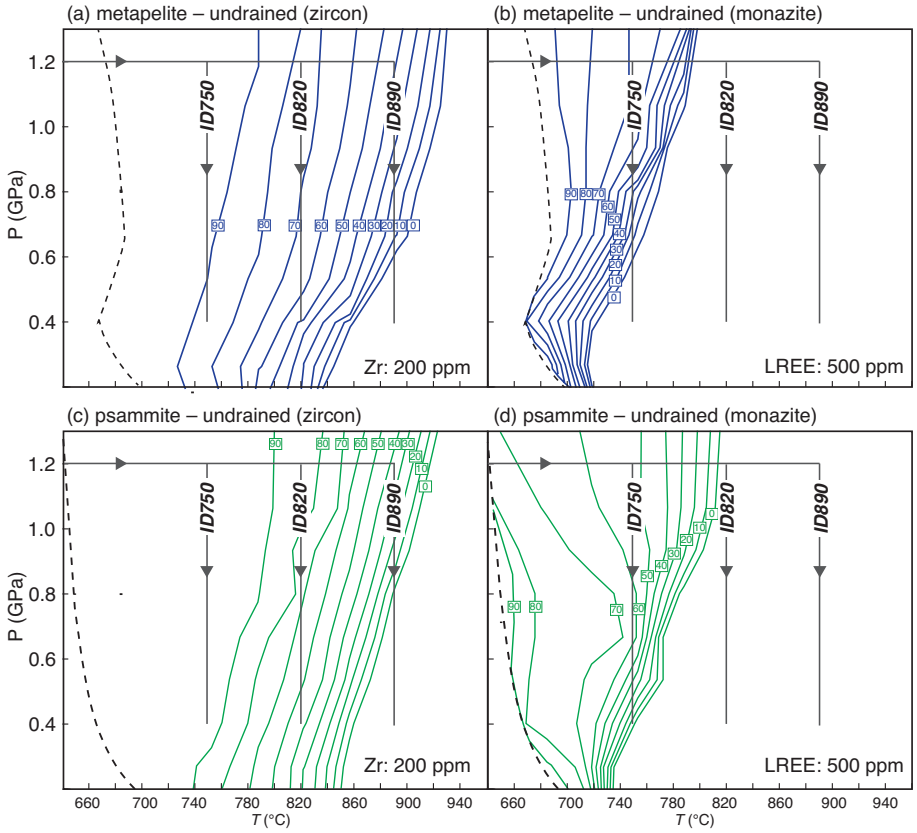

Fig. 4. *P–T* diagrams to show the stability of zircon and monazite during closed-system partial melting (modified from Kelsey *et al.* 2008). Contours represent the proportion of zircon or monazite remaining. The bold dashed line is the fluid-present solidus. In an undrained system, monazite is expected to be mostly or completely consumed during the *P–T* evolution. With the exception of the highest-temperature *P–T* path (ID890), most zircon is expected to survive.

for the psammite. In contrast, during isobaric heating, complete dissolution of monazite is predicted to occur within 120 °C of the fluid-present solidus for the metapelite (Fig. 4b) and within 180 °C for the psammite (Fig. 4d). During decompression, for the metapelite, all remaining monazite is consumed along path ID750 (Fig. 4c). For the psammite, *c.* 10% monazite survives after decompression along path ID750 (Fig. 4d). The dissolution contours for both zircon and monazite are more closely spaced at high temperature, which suggests that dissolution of these minerals is non-linear and increases with temperature. Because the system is undrained, after decompression both zircon and monazite will crystallize during cooling to the fluid-present solidus, as discussed by Kelsey *et al.* (2008).

Melt production in a drained (conditionally open) system

The *P–T* phase diagrams in Figure 1 are only appropriate for evaluating the amount of melt produced up to the melt connectivity transition at 7 mol%. *P–T* phase diagrams for progressively melt-depleted compositions are presented in Figures 2a and 3a for the pelite and Figures 2b and 3b for the greywacke. Each diagram comprises a series of panels that are calculated for incrementally melt-depleted bulk compositions along each *P–T* path. Each panel shows melt mol% isopleths and the stability field of major ferromagnesian minerals. Melt loss events are located on the seams between the panels. For the isobaric heating segment of the moderate-pressure *P–T* paths, phase diagram panels are stacked from low to high temperature, representing the initial protolith compositions and progressively more residual source compositions following melt loss events (Fig. 2a and b). For the decompression segment of the moderate-pressure *P–T* paths phase diagram panels are stacked from high to low pressure, representing progressively more residual source compositions following melt loss events (Fig. 2a and b). For the high-pressure *P–T* path for both rock types, the heating segment is shown by the panel in the low-*T*–high-*P* portion of the diagrams (Fig. 3a and b) and the isothermal decompression segment consists of a series of panels stacked from high to low pressure on the high-*T* portion of the diagrams (Fig. 3a and b).

Melt mol% isopleths are steeper for residual compositions compared with the original undrained bulk compositions (compare Fig. 1 with Figs 2 and 3). In some cases melt isopleths are negatively sloping for residual compositions (e.g. the pelite ID820 path in Fig. 2a), which indicates that decompression across these isopleths crystallizes melt. For the pelite and greywacke, the ID890 path crosses the solidus at *c.* 0.8 GPa. For the greywacke, the ID750 path crosses the solidus at 0.6 GPa and re-crosses it at 0.5 GPa owing to the up-temperature kink in the solidus (Fig. 2b).

The amount of melt generated along each *P–T* path for the drained situation is significantly less than the melt produced for the undrained situation. For the pelite in a drained system, the total amount of melt produced along the *P–T* paths ID750, ID820, ID890 and HP is 20, 28, 30 and 31 mol%, respectively, which is 6–28 mol% less than for the undrained situation (Yakymchuk & Brown 2014). For the greywacke in a drained system, the total amount of melt produced along the *P–T* paths ID750, ID820, ID890 and HP is 8, 20, 18 and 19 mol%, respectively, which is 3–24 mol% less than for the undrained situation (Yakymchuk & Brown 2014).

Zircon and monazite behaviour in a drained (conditionally open) system

The amounts of zircon and monazite dissolution are plotted along the corresponding *P–T* path segments, as summarized in Figures 5a

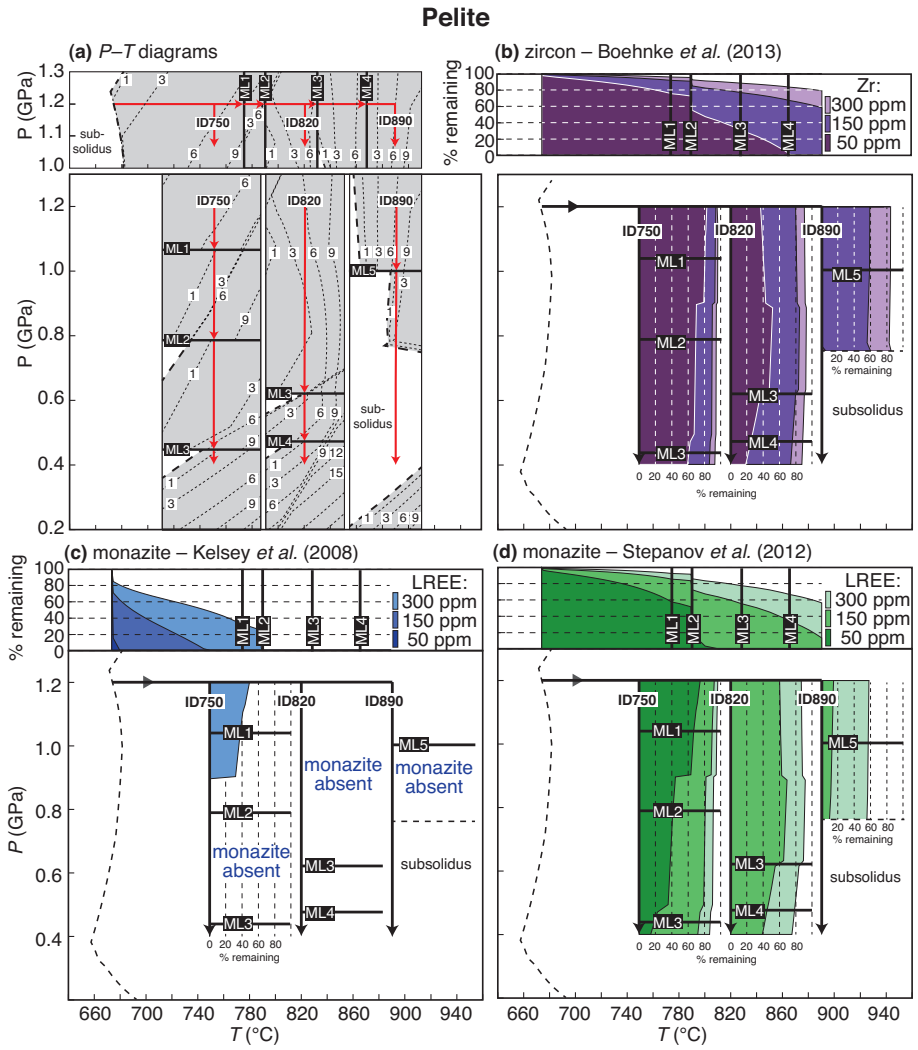

Fig. 5. (**a**) Composite *P–T* diagrams for conditionally open-system melting of a pelite along the moderate-pressure *P–T* paths (paths ID750, ID820 and ID890 in Fig. 1) simplified from Figure 2a. (**b–d**) *P–T* diagrams of the calculated proportion of zircon (**b**) and monazite (**c**, **d**) remaining during open-system melting of a pelite along the moderate-pressure *P–T* paths. Results are presented from the monazite solubility equations of Kelsey *et al.* (2008) in (**c**) and Stepanov *et al.* (2012) in (**d**). Three initial concentrations (50, 150 and 300 ppm) were modelled. It should be noted that the '% remaining' fields for the lower Zr and LREE concentrations cover portions of the fields for the higher concentrations. The dashed line is the fluid-present solidus. Most zircon is expected to survive the *P–T* evolution, except for protoliths with very low (50 ppm) initial Zr concentrations. Depending on the solubility equation used, monazite is expected to be completely (**c**) or mostly consumed (**d**) during the *P–T* evolution.

and 6a for the pelite and Figures 7a and 8a for the greywacke. These amounts are shown as plots of per cent remaining in Figures 5b–d and 6b–d for the pelite and Figures 7b–d and 8b–d for the greywacke for the range of starting concentrations of Zr and LREE (50, 150 and 300 ppm). In addition, the proportions of new zircon and monazite growth during isobaric cooling to the solidus at 0.7 and 0.4 GPa, normalized to the amount of zircon and monazite present at peak *T*, are shown in Figure 9 for the pelite and Figure 10 for the greywacke.

Some zircon is expected to survive heating and decompression for initial Zr concentrations of 150 and 300 ppm for both the pelite (Figs 5b and 6b) and greywacke (Figs 7b and 8b). For pelite with an initial Zr concentration of 150 ppm, along paths ID750, ID820, ID890 and HP the amount of zircon remaining at the end of each path is 87%, 73%, 59% and 40%, respectively. For a greywacke with an initial Zr concentration of 150 ppm, along paths ID750, ID820, ID890 and HP the amount of zircon remaining at the end of each path is 93%, 80%, 71% and 65%, respectively. For lower initial concentrations of Zr (50 ppm), the amount of zircon remaining is much less and is completely consumed along paths ID890 and HP for the pelite and path HP for the greywacke (Figs 5b, 6b and 8b).

Using the monazite solubility equation of Kelsey *et al.* (2008) monazite is predicted to be completely consumed along the low-temperature part of the prograde segment of most *P–T* paths modelled. For an initial LREE concentration of 150 ppm, during isobaric heating monazite is completely consumed at 750 °C for the pelite (Fig. 5c) and at 710 °C for the greywacke (Fig. 7c). For the lowest LREE concentration modelled (50 ppm), monazite is completely consumed within a few tens of degrees above the fluid-present solidus (Figs 5c and 7c). For the highest LREE concentration modelled (300 ppm), only the ID750 path for the greywacke has monazite (35%) that survives decompression (Fig. 7c).

The amount of monazite dissolution is significantly less using the solubility equation of Stepanov *et al.* (2012). In this case, monazite survives heating and high-*T* decompression in both the pelite and the greywacke, except for the lowest LREE concentration of 50 ppm. For isobaric heating to 890 °C and an initial LREE concentration of 150 ppm, 13% monazite remains for the pelite and 43% remains for the greywacke (Figs 5d and 7d). For pelite with an initial LREE concentration of 150 ppm along paths ID750, ID820 and ID890 the amount of monazite remaining is 71%, 39% and 14%, respectively (Fig. 5d), whereas monazite is completely consumed during decompression along the HP path (Fig. 6d). For the greywacke, the amount of monazite remaining at the end of paths ID750, ID820, ID890 and HP is 89%, 57%, 41% and 40%, respectively (Figs 7d and 8d).

During isobaric cooling to the solidus, the amount of new zircon growth in the source varies from <1% to *c*. 32% relative to the residual amount of zircon present in the pelite after isothermal decompression and from <1% to *c*. 52% relative to the residual

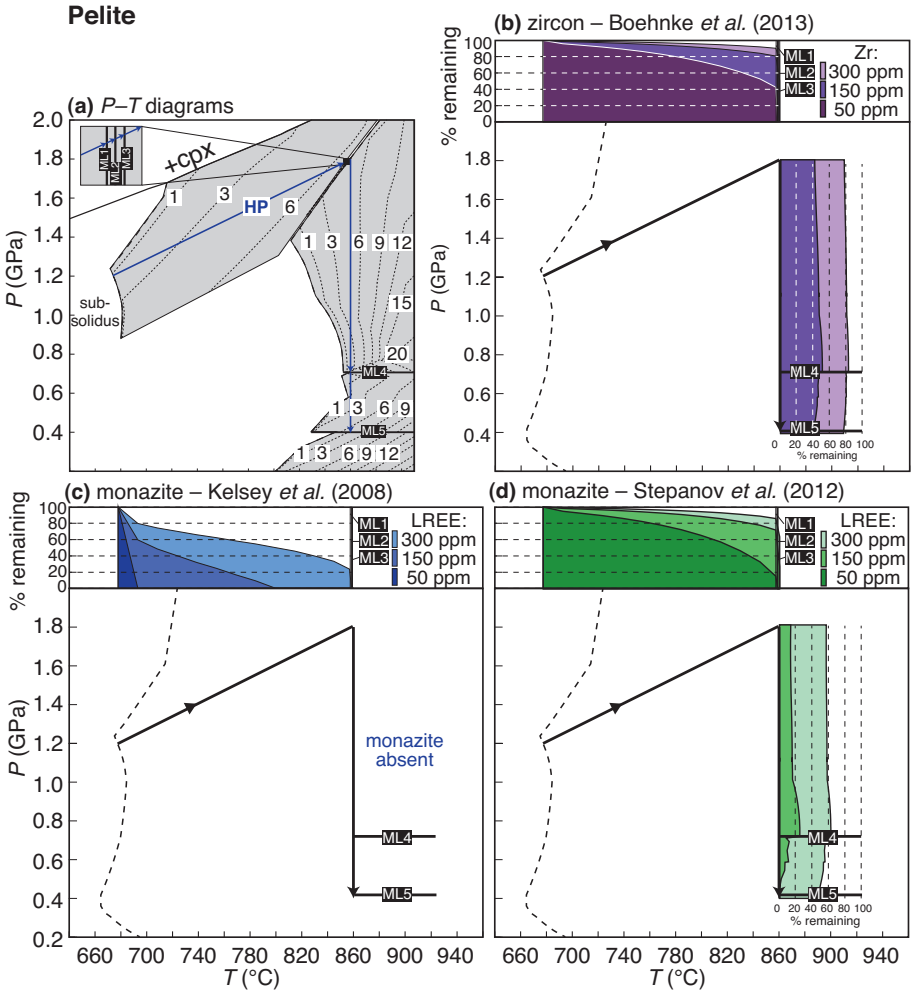

Fig. 6. (**a**) Composite *P–T* diagram for conditionally open-system melting of a pelite along the high-pressure *P–T* path (path HP in Fig. 1) simplified from Figure 3a. (**b–d**) *P–T* diagrams of the calculated proportion of zircon (**b**) and monazite (**c**, **d**) remaining during open-system melting of a pelite along the high-pressure *P–T* path. Results are presented from the monazite solubility equations of Kelsey *et al.* (2008) in (**c**) and Stepanov *et al.* (2012) in (**d**). Three initial concentrations (50, 150 and 300 ppm) were modelled. It should be noted that the '% remaining' fields for the lower Zr and LREE concentrations cover portions of the fields for the higher concentrations. The dashed line is the fluid-present solidus. Some zircon is expected to survive decompression, except for protoliths with low initial Zr concentrations, whereas monazite is expected to be mostly or completely consumed.

amount of zircon present in the greywacke (Figs 9 and 10). Similarly, using the Stepanov *et al.* (2012) dissolution equation, the amount of new monazite growth ranges from <1% to *c*. 35% for the pelite and from <1% to *c*. 50% for the greywacke relative to the residual amount of monazite present after isothermal decompression (Figs 9 and 10).

For protolith compositions with the lowest initial Zr and LREE concentrations there is a high proportion of new zircon and monazite relative to the inherited amount. However, the total amounts of zircon and monazite present at the elevated solidus after isobaric cooling are small relative to the initial quantity at the fluid-present solidus (compare Figs 5–8 and 9 and 10). The new zircon and monazite may occur as new grains, but are more likely to be present as significant overgrowths on residual cores. For higher initial Zr and REE concentrations, new growth during cooling to the solidus is predicted to be low in relation to the residual amount, and zircon and monazite grains are expected to contain large inherited cores with narrow rim overgrowths. In some cases, no new growth of zircon and monazite is expected during cooling because melt drainage has completely depleted the source in Zr and LREE. This is the case for monazite dissolution for most of the scenarios modelled using the Kelsey *et al.* (2008) dissolution equation.

In summary, except for very low (50 ppm) initial Zr concentrations, most zircon is likely to survive during prograde heating through the granulite facies. The amount of dissolution expected for monazite is very different according to which of the two solubility equations is used. Using the equation of Kelsey *et al.* (2008), monazite is completely consumed along the low-temperature part of all *P–T* paths for the pelite and along most *P–T* paths for the greywacke. In contrast, using the equation proposed by Stepanov *et al.* (2012), for lower LREE concentrations monazite may be consumed in both the pelite and the greywacke along all *P–T* paths, but for higher LREE concentrations some monazite is expected to survive. During cooling to the solidus from peak *T*, the amount of new zircon and monazite growth is expected to be limited in the melanosome.

Discussion

Limitations and assumptions

The limitations and assumptions of the method applied here to zircon and monazite dissolution have been discussed in detail by Kelsey *et al.* (2008), but are briefly described next for completeness. In addition to the inherent uncertainties in the zircon and monazite solubility equations of Kelsey *et al.* (2008), Stepanov *et al.* (2012) and Boehnke *et al.* (2013), the following assumptions apply to the modelling presented here: (1) all of the Zr and LREE required for saturation is contributed by dissolving zircon and monazite; (2) no zircon or monazite is sequestered away from the reaction volume, such as grains forming inclusions in major rock-forming minerals; (3) no Zr or LREE is partitioned into other minerals (e.g. Zr in rutile and/or garnet); (4) no zircon or monazite is produced as a result of the breakdown of Zr- and LREE-bearing minerals during the *P–T*

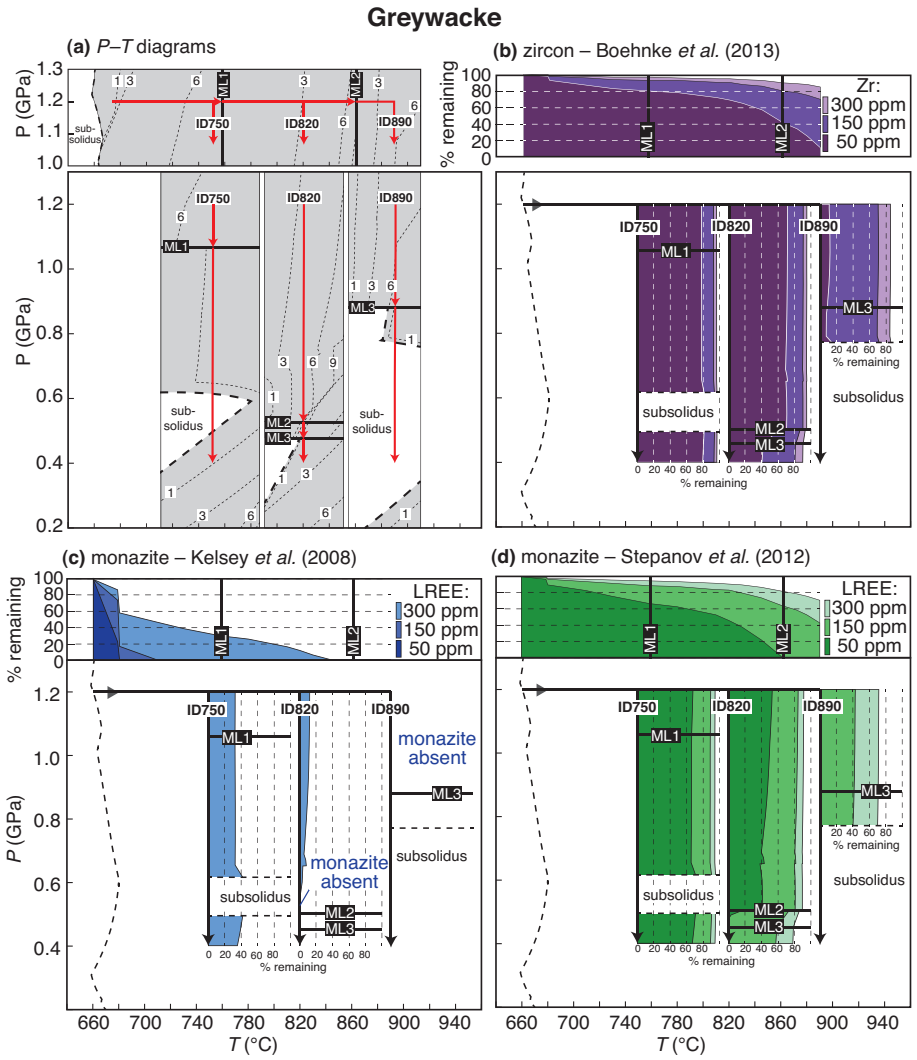

Fig. 7. (**a**) Composite *P–T* diagrams for conditionally open-system melting of a greywacke along the moderate-pressure *P–T* paths (paths ID750, ID820 and ID890 in Fig. 1) simplified from Figure 2b. (**b**–**d**) *P–T* diagrams of the calculated proportion of zircon (**b**) and monazite (**c**, **d**) remaining during open-system melting of a greywacke along the moderate-pressure *P–T* paths. Results are presented from the monazite solubility equations of Kelsey *et al.* (2008) in (**c**) and Stepanov *et al.* (2012) in (**d**). Three initial concentrations (50, 150 and 300 ppm) were modelled. It should be noted that the '% remaining' fields for the lower Zr and LREE concentrations cover portions of the fields for the higher concentrations. The dashed line is the fluid-present solidus. Except for protoliths with low initial Zr concentrations (50 ppm), most zircon is expected to survive the *P–T* evolution, whereas proportionally more monazite dissolution is predicted for higher-temperature *P–T* paths.

evolution; (5) both zircon and monazite are stoichiometric. In addition, for open-system behaviour, we assume that no zircon or monazite is entrained in the extracted melt.

The effects of some of these assumptions on the application of the results to natural examples are difficult to address except on a case-by-case basis. However, sequestration of zircon and monazite away from the reaction volume and partitioning of Zr or LREE into other minerals are problems in common to any application to migmatites and residual granulites. Sequestration of zircon or monazite away from the reaction volume or partitioning of Zr and LREE into major rock-forming minerals will decrease the 'effective' concentration of the source. For example, let us consider a rock with a bulk Zr concentration of 200 ppm. If one-quarter of the zircon by mass in the rock is sequestered away from the reaction volume as inclusions in major rock-forming minerals that do not participate in the partial melting reactions, a proportion consistent with the experimental and natural data reported by Watson *et al.* (1989), then the effective concentration of the source is 150 ppm Zr. In this case, the calculations presented in this study for 150 ppm Zr are appropriate for evaluating the proportion of zircon dissolution in this rock. Similarly, if 30 ppm Zr is partitioned into garnet (Kelsey & Powell 2011), and assuming no inclusion of zircon in rock-forming minerals, then the effective concentration of the source is 170 ppm Zr.

In nature, decompression would be isentropic rather than isothermal, unless heat is advected through the crust faster than the cooling rate during decompression (e.g. owing to ascending superheated melt), or unless the *P–T* path involves additional heating or cooling. Synchronous cooling and decompression would promote melt crystallization and zircon or monazite growth. By contrast, heating during decompression promotes increased dissolution of zircon or monazite. Therefore, the amounts of melt production and zircon or monazite dissolution are representative of the schematic decompression paths modelled and must be modified for application to natural decompression paths.

Source Zr and LREE depletion and enrichment during open-system melting

The extraction of Zr- and LREE-saturated melt has implications for the concentration of these elements in the source along the remainder of the *P–T* path. Extraction of melt with lower concentrations of Zr and LREE than the source will lead to relative enrichment of the source whereas loss of melt with higher concentrations will lead to relative depletion of the source (Rapp *et al.* 1987). The saturation values for Zr and LREE calculated along the prograde path at 1.2 GPa for the pelite and greywacke are compared with the source compositions in Figure 11.

The changes in the Zr concentrations of pelite and greywacke after incremental melt loss are shown in Figure 11a and b. Depending on the initial bulk-rock Zr concentration and the saturation concentration of

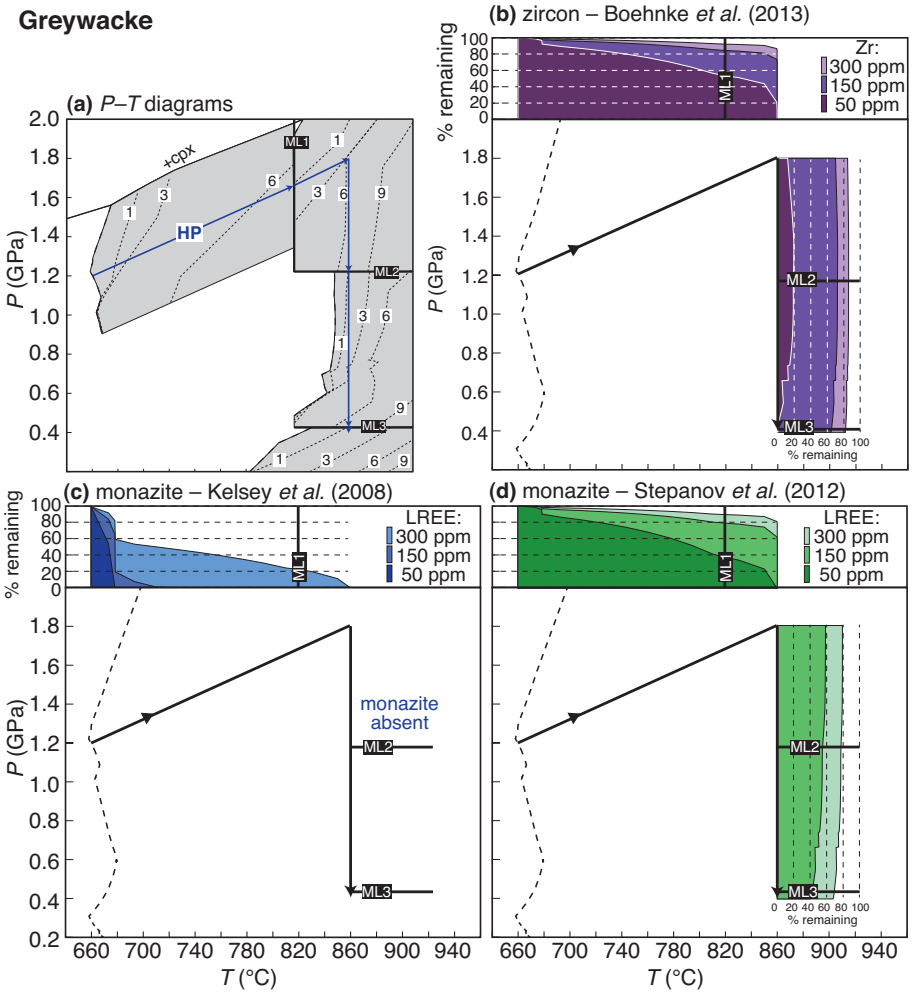

Fig. 8. (**a**) Composite *P–T* diagram for conditionally open-system melting of a greywacke along the high pressure *P–T* path (path HP in Fig. 1) simplified from Figure 3b. (**b**–**d**) *P–T* diagrams of the calculated proportion of zircon (**b**) and monazite (**c**, **d**) remaining during open-system melting of a greywacke along the high-pressure *P–T* path. Results are presented from the monazite solubility equations of Kelsey *et al.* (2008) in (**c**) and Stepanov *et al.* (2012) in (**d**). Three initial concentrations (50, 150 and 300 ppm) were modelled. It should be noted that the '% remaining' fields for the lower Zr and LREE concentrations cover portions of the fields for the higher concentrations. The dashed line is the fluid-present solidus. Most zircon is expected to survive heating and decompression, except for protoliths with low initial Zr concentrations, whereas monazite is predicted to be mostly consumed, except for protoliths with high initial LREE concentrations.

the melt, the source may become enriched or depleted in Zr. For example, let us consider a starting composition of 150 ppm for the pelite (Fig. 11a). At each melt loss event, the extracted melt has a greater concentration of Zr (176, 180, 221, 286 ppm) than the source (Fig. 11a). This results in the progressive depletion of the source in Zr. In contrast, for a pelite with an initial composition of 300 ppm Zr, at each melt loss event the extracted melt has a lower concentration of Zr than the source. This leads to incremental source enrichment (Fig. 11a).

Source depletion is most pronounced for pelite and greywacke with starting concentrations of 50 ppm Zr. At each melt loss event along the isobaric heating path, the melt is always relatively enriched in Zr compared with the source (Fig. 11a and b), which leads to its incremental depletion. At the end of the isobaric heating path at 890 °C, the concentration of Zr is expected to be *c.* 5 ppm for the pelite (Fig. 11a) and *c.* 30 ppm for the greywacke (Fig. 11b).

The concentration of LREE in the saturated melt is higher than the range of initial protolith concentrations modelled at each melt loss event (Fig. 11c and d), with the exception of LREE concentrations >260 ppm for the greywacke prior to ML1 (Fig. 11d). This results in the progressive depletion of the source in LREE for most natural LREE concentrations, and during open-system melting the concentration of LREE in the source almost always decreases after each melt loss event. A consequence of the lower effective LREE concentration is that more monazite is required to dissolve to saturate the melt during open-system melting than during closed-system behaviour, where the effective bulk concentration remains constant (Kelsey *et al.* 2008).

In nature the melt may be undersaturated in Zr and LREE if there is insufficient time for melt–residue equilibration prior to melt drainage (Watt *et al.* 1996). Thus, care is required in applying our results directly to natural examples. This is discussed further below.

Zr and LREE undersaturation in granites and leucosomes

In this study, melt is assumed to be saturated in Zr and LREE along the *P–T* path, as expected based on experimental data (Watson & Harrison 1983; Rapp & Watson 1986; Stepanov *et al.* 2012; Boehnke *et al.* 2013). However, leucosomes in migmatites and anatectic granites are commonly undersaturated in Zr and LREE when compared with protolith compositions (Bea *et al.* 1994; Ayres & Harris 1997; Zeng *et al.* 2005*a*,*b*,*c*). Furthermore, melanosomes in migmatites and residual granulites that have experienced melt loss do not show the drastic depletion of Zr and LREE that may be expected from the drainage of saturated melt (Sawyer 1986; Sawyer & Barnes 1988; Bea & Montero 1999; Solar & Brown 2001; Guernina & Sawyer 2003; Villaseca *et al.* 2003, 2007; Korhonen *et al.* 2010*b*).

Undersaturation of melt in Zr and LREE is unlikely to be due to inhibited accessory mineral dissolution during partial melting in the source based on the experimental data (Harrison & Watson 1983; Rapp & Watson 1986). If accessory mineral dissolution is not inhibited, then melting and melt extraction must have occurred faster than mineral–melt equilibration to generate undersaturated melt compositions, which is considered to be possible in migmatite

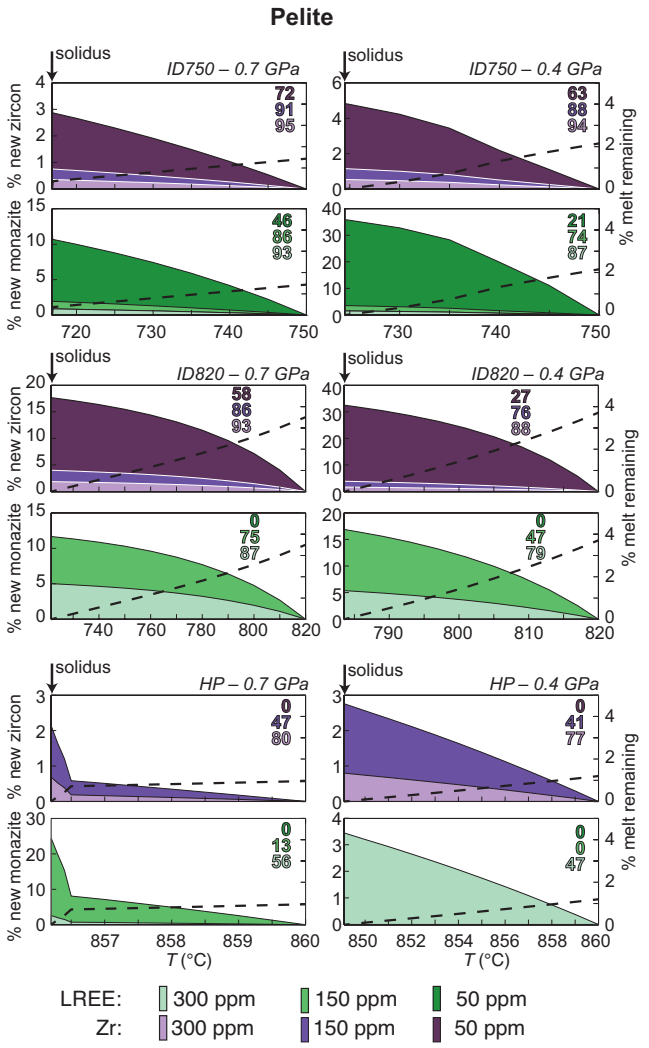

Fig. 9. Temperature–proportion diagrams for zircon, monazite and melt in pelite during cooling from the decompression segment of the *P–T* path to the solidus. The proportion of new zircon and monazite growth calculated relative to the amount of zircon and monazite present at the beginning of cooling is shown as shaded fields for three protoliths with initial Zr and LREE concentrations of 50, 150 and 300 ppm, respectively. The shaded numbers in the top-right corner of each plot represent the percentage of zircon and monazite at the solidus relative to starting amounts at the fluid-present solidus at the beginning of the *P–T* paths modelled (Figs 5 and 6). It should be noted that the fields for the higher Zr and LREE concentrations cover portions of the fields for the lower concentrations. The proportion of monazite was calculated using the Stepanov *et al.* (2012) solubility equation. The bold dashed line represents the amount of melt remaining (scale on the right-hand side of each plot). In general, the amount of new zircon and monazite crystallization is small. For protoliths with low initial Zr and LREE concentrations, the proportions of new zircon and monazite relative to the remaining zircon and monazite are greater than in protoliths with higher initial concentrations, but this simply reflects the fact that the proportion of residual zircon and monazite at the end of any *P–T* path is much less for these protoliths.

terranes that have undergone strong syn-anatectic deformation where melt escape is expected to be more rapid (Sawyer 1991; Watt & Harley 1993; Watt *et al.* 1996).

Another factor may be the proportion of accessory minerals sequestered in the major rock-forming minerals (Watson *et al.* 1989; Bea 1996). Until the stability of the host minerals is exceeded, the Zr and LREE budget of the source rocks will be dominated by accessory mineral grains in the rock matrix (Watson *et al.* 1989). The stability of these host minerals is controlled by the bulk composition of the rock and the *P–T* conditions of metamorphism. Fortunately, the stability of the common rock-forming minerals is well constrained for most clastic metasedimentary rocks up to UHT conditions (Johnson *et al.* 2008; Brown & Korhonen 2009).

A likely host for zircon and monazite in high-grade metamorphic rocks is biotite. Biotite is used in the following example because its proportion decreases with increasing temperature above the stability field of muscovite in most pelites and greywackes. However, we acknowledge that biotite is not the only potential host for zircon and monazite during prograde metamorphism. As biotite is consumed during fluid-absent melting accessory minerals may be liberated to allow interaction with the melt, which should yield leucosomes and anatectic granites with concentrations of these elements closer to saturation values, or, if significant accessory minerals are entrained in the melt, even supersaturated concentrations (Brown 2013). A possible example of supersaturation occurs in migmatite from the southern Appalachian orogen where very high Zr concentrations were measured in leucosome; this was attributed to the physical concentration of newly crystallized zircon by inclusion in peritectic plagioclase and garnet during biotite breakdown (Moecher *et al.* 2004).

In clastic metasedimentary rocks biotite is consumed during melting to produce peritectic garnet at high *P*, cordierite at low *P*, or orthopyroxene at low *P* and high *T* (Fig. 1; also see Yakymchuk & Brown 2014). For the *P–T* paths modelled at 1.2 GPa in this study, the effects of accessory mineral sequestration are expected to be most important for $T<790$ °C for the pelite (Fig. 12a) and <780 °C for the greywacke (Fig. 12b) where the proportion of biotite does not change significantly. For the higher temperature paths, as biotite is consumed, at $T>790$ °C for the pelite and at $T>780$ °C for the greywacke, any zircon and monazite sequestered in biotite will become progressively available for reaction. However, the peritectic products of the incongruent melting reaction (e.g. garnet in Fig. 12) may sequester accessory minerals and may also partition trace elements versus melt. Thus, with increasing temperature garnet may concentrate an increasing amount of Zr, and K-feldspar and plagioclase may concentrate an increasing amount of LREE than at lower metamorphic grades (Fraser *et al.* 1997; Villaseca *et al.* 2003, 2007). As a result Zr and LREE liberated from the breakdown of accessory minerals may not all enter the melt but some may partition into peritectic minerals. Zirconium may also be partitioned into rutile in high-pressure granulites (Zack *et al.* 2004; Tomkins *et al.* 2007; Ewing *et al.* 2013). There has been some progress in modelling the partitioning of Zr between zircon, melt, garnet and rutile during anatexis of crustal rocks (Kelsey & Powell 2011; Skrzypek *et al.* 2012), but our understanding of the suprasolidus behaviour of the LREE is still limited.

A potentially important factor that may control the amount of zircon and monazite dissolution within a given time frame may be the crystal size distribution inherited from the subsolidus protolith (Nemchin & Bodorkos 2000). Nemchin *et al.* (2001) coupled a numerical model for Ostwald ripening with zircon morphology and zoning data from the Tickalara metamorphic rocks in Australia to suggest that, in the presence of melt, smaller zircon grains were preferentially dissolved and then new zircon was precipitated on the crystal faces of larger grains. When present smaller grains will preferentially contribute Zr to the melt, which increases the preservation potential of the larger grains. In the absence of smaller grains, dissolution of the larger grains is needed to saturate the melt in Zr. The time required for complete dissolution of larger grains of

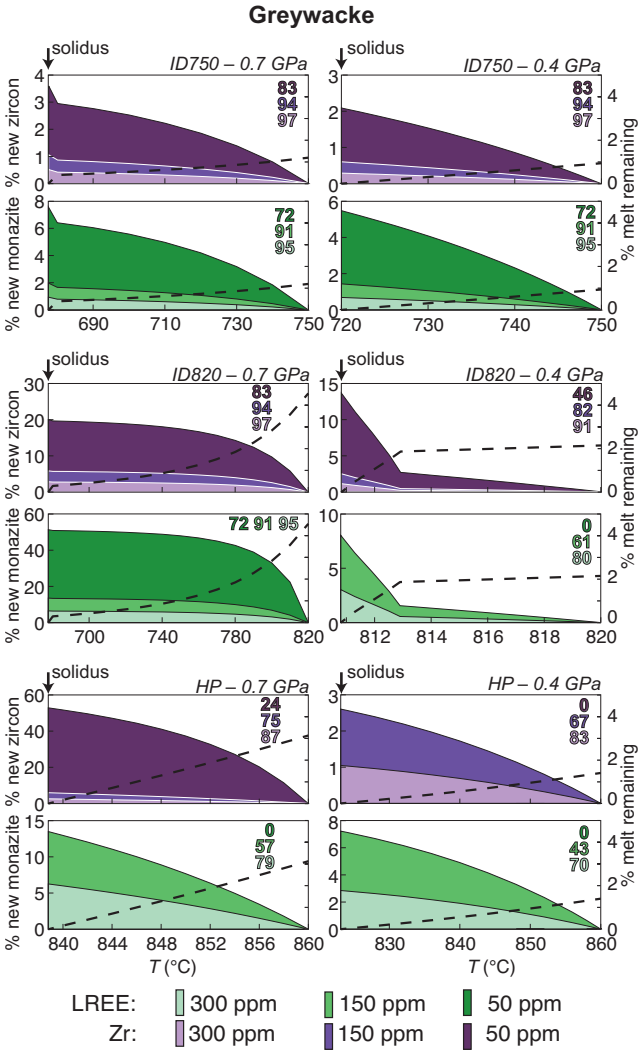

Fig. 10. Temperature–proportion diagrams for zircon, monazite and melt in greywacke during cooling from the decompression segment of the *P–T* path to the solidus. The proportion of new zircon and monazite growth calculated relative to the amount of zircon and monazite present at the beginning of cooling is shown as shaded fields for three protoliths with initial Zr and LREE concentrations of 50, 150 and 300 ppm, respectively. The shaded numbers in the top-right corner of each plot represent the percentage of zircon and monazite at the solidus relative to starting amounts at the fluid-present solidus at the beginning of the *P–T* paths modelled (Figs 7 and 8). It should be noted that the fields for the higher Zr and LREE concentrations cover portions of the fields for the lower concentrations. The proportion of monazite was calculated using the Stepanov *et al.* (2012) solubility equation. The bold dashed line represents the amount of melt remaining (scale on the right-hand side of each plot). In general, the amount of new zircon and monazite growth is small. For protoliths with low initial Zr and LREE concentrations, the proportions of new zircon and monazite growth relative to the remaining zircon and monazite are greater than in protoliths with higher initial concentrations, but this simply reflects the fact that the proportion of residual zircon and monazite at the end of any *P–T* path is much less for these protoliths.

zircon (and monazite) is significantly longer than for smaller grains. For example, for zircon grains with a diameter of 200 μm the time required for complete dissolution is >1 order of magnitude larger than for grains with a diameter of 50 μm (Harrison & Watson, 1983), whereas for monazite grains with a diameter of 50 μm, the time required for complete dissolution is >2.5 orders of magnitude longer than for grains with a diameter of 5 μm (Rapp & Watson 1986). Therefore, the pre-anatectic crystal size distribution may have important consequences for the preservation of inherited zircon (and monazite).

Consequences of monazite dissolution for Sm–Nd isotopes in granites

The Sm–Nd isotope system is commonly used to link granites emplaced in the upper crust to their sources in the deep crust. The amount of dissolution or entrainment of apatite and monazite in melt may modify the Nd-isotope ratio so that the leucosome is either more or less radiogenic than the source. This has been documented in Himalayan leucogranites (Ayres & Harris 1997), the Goat Ranch migmatite complex associated with the Sierra Nevada batholith (Zeng *et al.* 2005*a*,*b*,*c*) and the Fosdick migmatite–granite complex in West Antarctica (Korhonen *et al.* 2010*b*). Leucosome with less radiogenic Nd-isotope values is consistent with monazite dissolution and inhibited apatite dissolution, possibly in relatively low-temperature melts where water content is relatively high. Melt with relatively high water content favours monazite dissolution whereas apatite dissolution is independent of water content (Harrison & Watson 1983). Leucosomes with more radiogenic values than the source are attributed to a larger contribution of apatite dissolution and a lesser contribution from monazite.

In this study, monazite is predicted to dissolve along the prograde path (Figs 5–8) and is either completely or mostly consumed by 890 °C according to the particular solubility equation used. The decreased proportion of monazite available at high temperature may enhance the dissolution of apatite to provide the LREE needed for saturation. Furthermore, relatively little melt production or accessory mineral dissolution is predicted during decompression compared with heating, which indicates that disequilibrium of Nd isotopes between the source and the melt is most likely to record prograde metamorphism rather than decompression.

Distribution of heat-producing elements in the crust

The decay of radioactive elements in the thickened continental crust is one of the principal sources of heat for regional metamorphism, particularly for granulite and UHT metamorphism (Clark *et al.* 2011). In the continental crust, accessory minerals such as zircon and monazite are important hosts for the radioactive elements thorium and uranium. Contributions to the radiogenic heat flux of the Earth from the decay of potassium were important in the Archaean but have become less so over time (Arevalo *et al.* 2009). Therefore, the distribution of zircon and monazite in the crust has important implications for the partitioning of heat-producing elements throughout the crust.

Whole-rock chemical data from low- and high-grade rocks in the Ivrea Zone (kinzigites versus stronalites) have been used to suggest that geochemical changes accompanying partial melting and melt extraction have only a minor influence on the distribution of heat-producing elements in the deep crust (Bea & Montero 1999). This contrasts with the view that there is a secular change in the distribution of heat-producing elements in different levels of the crust (Sandiford & McLaren 2002; Sandiford *et al.* 2002) and that there is a significant depletion of these elements in the deep crust compared with the upper crust (Rudnick & Gao 2003). The latter view is supported by the results of this study, which suggest that zircon and monazite are expected to be partially to completely dissolved during high-*T* metamorphism and the extraction of this melt will deplete the residue in these elements.

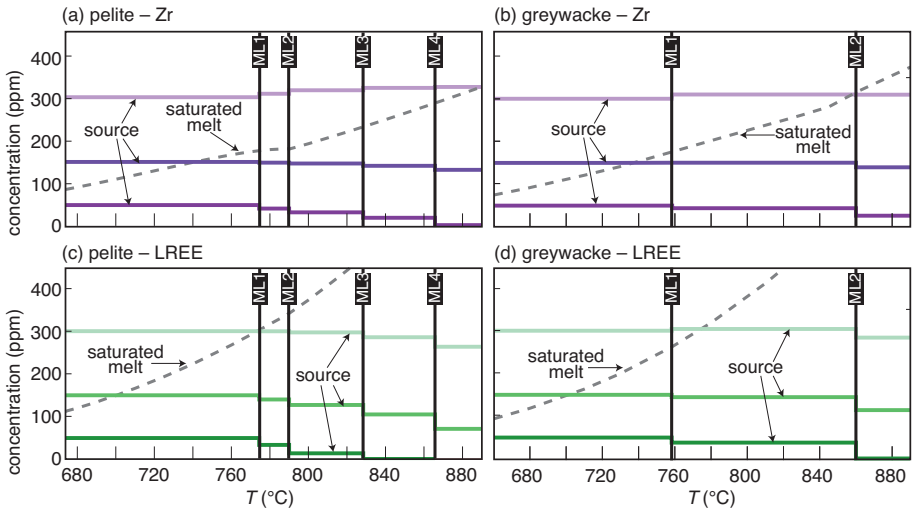

Fig. 11. Concentrations of the Zr and LREE in the source and melt for conditionally open-system behaviour along an isobaric heating path at 1.2 GPa for pelite (**a**, **c**) and greywacke (**b**, **d**). The concentrations of these elements in the source change in a stepwise fashion after each melt loss event. The saturation concentration of the melt is shown by the dashed curve. Extraction of saturated melt with higher Zr or LREE concentrations than the source will deplete the source in these elements. In these cases, proportionally more zircon and monazite dissolution is required to saturate the melt for the remainder of the heating path.

One possible explanation for this discrepancy in the Ivrea Zone might be that melt extraction was sufficiently fast that the melt was severely undersaturated in Zr and LREE. However, based on the calculations of Harrison & Watson (1983) and Rapp & Watson (1986) for water-undersaturated melts, time scales for melt extraction have to be significantly less than 1000 years. Alternatively, the stronalites could represent a mix of residue, crystallized *in situ* melt and early crystallized cumulates formed from melt transferring from the deeper crust (e.g. Brown 2010; Korhonen *et al.* 2013*b*; Morfin *et al.* 2013; Yakymchuk *et al.* 2013). In support of the second explanation, we note that metasedimentary diatexites from the Ivrea Zone contain more quartz and feldspar than expected from phase equilibria modelling, which suggests that these rocks represent melt accumulation zones or that melt escape was inefficient (Redler *et al.* 2013).

Interpreting accessory mineral ages

As discussed above, the factors that control zircon and monazite dissolution and growth in suprasolidus rocks are complex and the significance of U–Pb ages retrieved from them should be assessed on a case-by-case basis. However, some general conclusions may be drawn from the modelling presented in this study.

Except for very low whole-rock concentrations of Zr, some zircon is expected to survive high-*T* metamorphism and partial melting. In contrast, except for highest LREE concentrations modelled, pre-existing subsolidus monazite is expected to be less abundant in the source than zircon, but monazite is expected to be more abundant in leucosomes and granites. Furthermore, for rocks with average concentrations of Zr and LREE only limited new growth of zircon and monazite is expected to have occurred in melanosomes in migmatites or in residual granulites during cooling to the solidus. These results are consistent with the study of Williams (2001), who documented the morphology and determined the age of zircon and monazite growth in migmatites from the Cooma complex of southeastern Australia. Williams (2001) noted that in melanosomes most zircon survived the prograde evolution and became surrounded by thin overgrowths during cooling to the solidus, whereas in leucosomes more prismatic zircon mostly represents new growth. By contrast, subsolidus monazite mostly vanished from the rock during the prograde evolution and inherited cores are scarce (Williams 2001); new monazite is more abundant in leucosomes than in melanosomes, as would be expected from this study.

Zircon and monazite have similar closure temperatures for Pb for similar grain sizes and cooling rates (Cherniak *et al.* 2004). However, a common observation in high-grade metamorphic rocks is that zircon yields older ages than monazite, although there are exceptions (Korhonen *et al.* 2013*a*). A possible explanation is that zircon and monazite growth during cooling is non-linear and growth rates are expected to be higher at initial supersaturation, which may occur at higher temperatures for zircon (Kelsey *et al.* 2008; Fig. 4). The results of this study support non-linear rates of zircon and monazite growth during cooling (Figs 9 and 10), but we emphasize that this rate is proportional to the change in the amount of melt. In addition, the effective Zr and LREE bulk-rock concentrations have a strong control on the amount of new zircon and monazite growth (Figs 9 and 10).

The timing of events and the rates of tectonometamorphic processes operating in the deep crust rely on the correct interpretation of ages retrieved from accessory minerals. In migmatites and residual granulites, intrasample ranges of concordant U–Pb zircon ages and intersample variation in weighted mean ages within a single metamorphic event complicate the interpretation of age data (Reno *et al.* 2012; Korhonen *et al.* 2013*a*). Let us consider, for example, whether ranges of concordant ages in depleted source rocks record the duration of a process such as crustal melting or simply register the time taken for melt trapped by the percolation threshold to crystallize during exhumation and cooling. To distinguish between these interpretations it may be necessary to evaluate the oxygen isotope composition of zircon in addition to U–Pb age data. For example, Jeon *et al.* (2012) used the difference in oxygen isotope compositions and U–Pb ages of zircon cores and rims from granites in eastern Australia to constrain the timing of crustal recycling to less than 15 Ma.

In migmatites and granulites, we might ask whether weighted mean ages record the timing of final crystallization of trapped melt at the solidus and, if so, whether differences in weighted mean ages between samples represent variations in the solidus temperature according to the degree of melt depletion. In variably depleted source rocks that record a range of suprasolidus *P*–*T* conditions, a range of concordant U–Pb ages from matrix zircon grains is likely to register the time taken for melt trapped on grain boundaries to crystallize during cooling to the solidus. However, given the non-linear rate of zircon growth during cooling (Watson 1996; Harrison *et al.* 2007; Kelsey *et al.* 2008; this study), weighted mean ages may not represent the timing of final crystallization of trapped melt close to the solidus unless the solidus is very elevated. Williams (2001) also noted that monazite in both melanosomes and leucosomes grew in two stages: rapidly at first, trapping inclusions of

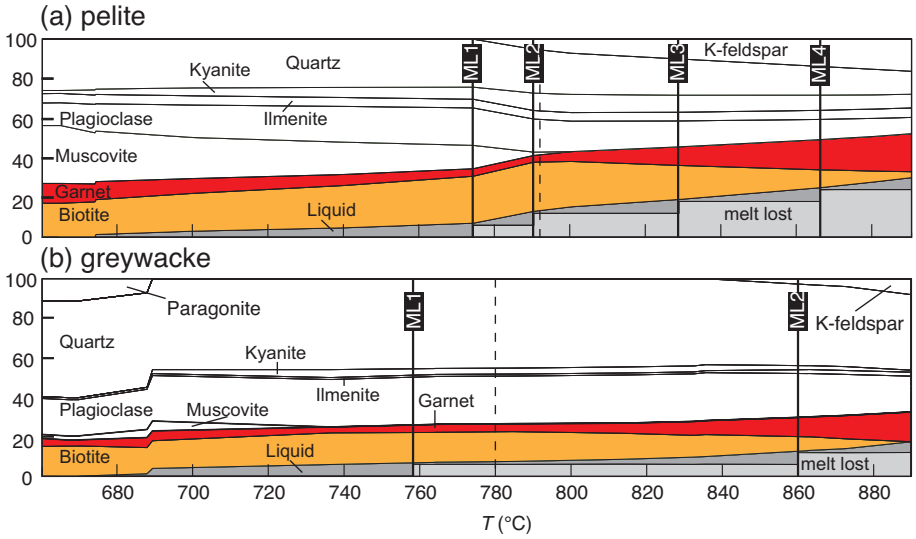

Fig. 12. Molar proportions of phases plotted against temperature for conditionally open-system behaviour along an isobaric heating path at 1.2 GPa for pelite (**a**) and greywacke (**b**). The vertical dashed lines represent the temperatures at which the proportion of biotite decreases significantly during heating owing to fluid-absent hydrate-breakdown melting. Because biotite is a common host for zircon and monazite, the breakdown of biotite during heating above these temperatures will liberate these minerals and make them available for reaction with melt.

melt and aluminosilicate, and then more slowly. Based on the modelling reported here, the proposal by Korhonen *et al.* (2013*a*) that differences in weighted mean ages among samples from ultrahigh-temperature granulites from the Eastern Ghats Province most probably represent variations in the solidus temperature according to the degree of melt depletion seems reasonable.

For matrix monazite grains, U–Pb monazite ages retrieved from source rocks are predicted to record new growth during cooling to the solidus. However, given the different saturation curves for Zr and LREE (Fig. 11), this monazite is likely to have grown closer to the solidus than zircon and, as a result, weighted mean ages are more likely to register the timing of final crystallization of trapped melt close to the solidus. Furthermore, differences in weighted mean ages among samples are very likely to represent variations in the solidus temperature according to the degree of melt depletion (Reno *et al.* 2012; Korhonen *et al.* 2013*a*).

One last issue to consider is that of suprasolidus prograde growth as argued in several studies, some of which are discussed below. Based on the results of this study, it is hard to understand how zircon may grow during the suprasolidus prograde evolution except as a result of Ostwald ripening (Nemchin *et al.* 2001). It is intrinsically difficult to distinguish prograde from retrograde zircon growth in the presence of anatectic melt, even where REE partitioning data and Ti-in-zircon thermometry are used in combination with geochronology (Baldwin & Brown 2008).

In the case of the Val Malenco granulites, which are located in northern Italy, Hermann & Rubatto (2003) linked the first stage of new zircon growth to the beginning of fluid-absent muscovite-breakdown partial melting. Although those researchers did not explicitly discuss the mechanism of growth of new zircon, we suggest that melt-enhanced Ostwald ripening may have been responsible for the first-stage overgrowth that trapped prograde muscovite and K-feldspar, and also biotite, as inclusions against inherited cores of zircon.

In the Ivrea–Verbano Zone of northern Italy, Ewing *et al.* (2013) have recently shown that the age of the regional granulite-facies metamorphism was *c.* 316 Ma, older than determined by Vavra *et al.* (1996) at *c.* 296 Ma, which calls into question the interpretation of prograde growth of zircon as proposed by Vavra *et al.* (1996). Because Vavra *et al.* related the different types of zoning in sequential overgrowths on inherited cores in zircon to growth in the presence of anatectic melt, we infer that this zircon more probably represents growth during cooling to the solidus. As recognized in both studies, the zircon morphologies are complex and partly reflect younger recrystallization of pre-existing zircon in the presence of fluid.

At Mount Stafford in central Australia, many of the features ascribed to prograde growth of zircon and monazite (Rubatto *et al.* 2006) are also compatible with growth during cooling from the metamorphic peak to the solidus. Examples include core–rim structure in monazite marked by subtle age differences, which could reflect variation in monazite saturation, and an increasing Eu anomaly in monazite co-precipitating with K-feldspar, which could occur during melt crystallization. The microstructure of these migmatites is extremely complex, with patchy distribution of minerals and multiple assemblages within any one thin section (White *et al.* 2003), making interpretations ambiguous. In particular, the occurrence of idioblastic K-feldspar and garnet is equally consistent with peritectic production or crystallization from melt, and it is unclear whether these minerals are late prograde or early retrograde, or, if both occur, how much of each type is present (White *et al.* 2003). Although these issues suggest caution in accepting an interpretation of prograde growth, given the short time scale for the regional-scale metamorphism in this area, the age of *c.* 1.8 Ga surely records the metamorphic peak within uncertainty.

Conclusions

Results of phase equilibria modelling of open-system melting of pelite and greywacke suggest that zircon is expected to survive the prograde evolution to peak temperature and subsequent isothermal decompression in both protoliths, whereas monazite may be mostly consumed. Melt loss from the residue is expected to progressively deplete the source of Zr and LREE, which may enhance the dissolution of zircon and monazite during heating to the metamorphic peak. Newly formed zircon and monazite are expected to be scarce in residues but more abundant in leucosomes in migmatites and in anatectic granites. Although there are many complicating factors, including mineral sequestration and partitioning of Zr and LREE between peritectic minerals and melt, the phase equilibria modelling of zircon and monazite behaviour during open-system melting presented here improves upon previous studies that were largely restricted to closed-system melting. Thus, this study provides a better framework within which to relate the U–Pb ages of accessory minerals to *P–T* paths, with the ultimate goal of better constraining the timing of events and the rates of tectonometamorphic processes during orogenesis.

This material is based upon work supported by the National Science Foundation under Grant No. ANT0944615 to M.B. This work has benefited from discussions with F. J. Korhonen and helpful comments by reviewer D. E. Kelsey. We thank J. F. A. Diener and N. M. Kelly for reviews of an earlier version of this work when it formed part of a larger paper, and C. Clark for his editorial handling. None the less, the authors are responsible for any misinterpretations or omissions that may persist.

References

Ague, J.J. 1991. Evidence for major mass-transfer and volume strain during regional metamorphism of pelites. *Geology*, **19**, 855–858.

Arevalo, R., Jr., McDonough, W.F. & Luong, M. 2009. The K/U ratio of the silicate Earth: Insights into mantle composition, structure and thermal evolution. *Earth and Planetary Science Letters*, **278**, 361–369.

Ayres, M. & Harris, N. 1997. REE fractionation and Nd-isotope disequilibrium during crustal anatexis: Constraints from Himalayan leucogranites. *Chemical Geology*, **139**, 249–269.

Baldwin, J. & Brown, M. 2008. Age and duration of ultrahigh-temperature metamorphism in the Anápolis–Itauçu Complex, Southern Brasília Belt, central Brazil—constraints from U–Pb geochronology, mineral rare earth element chemistry and trace-element thermometry. *Journal of Metamorphic Geology*, **26**, 213–233.

Bea, F. 1996. Residence of REE, Y, Th and U in granites and crustal protoliths; implications for the chemistry of crustal melts. *Journal of Petrology*, **37**, 521–552.

Bea, F. & Montero, P. 1999. Behavior of accessory phases and redistribution of Zr, REE, Y, Th, and U during metamorphism and partial melting of metapelites in the lower crust: An example from the Kinzigite Formation of Ivrea–Verbano, NW Italy. *Geochimica et Cosmochimica Acta*, **63**, 1133–1153.

Bea, F., Pereira, M. & Stroh, A. 1994. Mineral/leucosome trace-element partitioning in a peraluminous migmatite (a laser ablation-ICP-MS study). *Chemical Geology*, **117**, 291–312.

Bea, F., Montero, P. & Ortega, M. 2006. A LA–ICP–MS evaluation of Zr reservoirs in common crustal rocks: Implications for Zr and Hf geochemistry, and zircon-forming processes. *Canadian Mineralogist*, **44**, 693–714.

Boehnke, P., Watson, E.B., Trail, D., Harrison, T.M. & Schmitt, A.K. 2013. Zircon saturation re-revisited. *Chemical Geology*, **351**, 324–334.

Brown, M. 2010. Melting of the continental crust during orogenesis: The thermal, rheological, and compositional consequences of melt transport from lower to upper continental crust. *Canadian Journal of Earth Sciences*, **47**, 655–694.

Brown, M. 2013. Granite: From genesis to emplacement. *Geological Society of America Bulletin*, **125**, 1079–1113.

Brown, M. & Korhonen, F.J. 2009. Some remarks on melting and extreme metamorphism of crustal rocks. *In*: Gupta, A.K. & Dasgupta, S. (eds) *Physics and Chemistry of the Earth's Interior*. Indian National Science Academy, Springer (India), New Delhi, 67–87.

Cherniak, D.J., Watson, E.B., Grove, M. & Harrison, T.M. 2004. Pb diffusion in monazite: A combined RBS/SIMS study. *Geochimica et Cosmochimica Acta*, **68**, 829–840.

Clark, C., Fitzsimons, I.C., Healy, D. & Harley, S.L. 2011. How does the continental crust get really hot? *Elements*, **7**, 235–240.

Clemens, J.D. 2006. Melting of the continental crust: Fluid regimes, melting reactions, and source-rock fertility. *In*: Brown, M. & Rushmer, T. (eds) *Evolution and Differentiation of the Continental Crust*. Cambridge University Press, Cambridge, 297–331.

Degeling, H., Eggins, S. & Ellis, D. 2001. Zr budgets for metamorphic reactions, and the formation of zircon from garnet breakdown. *Mineralogical Magazine*, **65**, 749–758.

Ewing, T.A., Hermann, J. & Rubatto, D. 2013. The robustness of the Zr-in-rutile and Ti-in-zircon thermometers during high-temperature metamorphism (Ivrea–Verbano Zone, northern Italy). *Contributions to Mineralogy and Petrology*, **165**, 757–779.

Fraser, G., Ellis, D. & Eggins, S. 1997. Zirconium abundance in granulite-facies minerals, with implications for zircon geochronology in high-grade rocks. *Geology*, **25**, 607–610.

Guernina, S. & Sawyer, E.W. 2003. Large-scale melt-depletion in granulite terranes: An example from the Archean Ashuanipi Subprovince of Quebec. *Journal of Metamorphic Geology*, **21**, 181–201.

Handy, M., Mulch, A., Rosenau, M. & Rosenberg, C. 2001. The role of fault zones and melts as agents of weakening, hardening and differentiation of the continental crust: A synthesis. *In*: Doyle, P., Hartley, A.J., Holdsworth, R.E., Morton, A.C., Stoker, M.S. & Turner, J. (eds) *The Nature and Tectonic Significance of Fault Zone Weakening*. Geological Society, London, Special Publications, **186**, 305–332.

Harley, S.L. 1998. On the occurrence and characterization of ultrahigh-temperature crustal metamorphism. *In*: Treloar, P.J. & O'Brien, P.J. (eds) *What Drives Metamorphism and Metamorphic Reactions?* Geological Society, London, Special Publications, **138**, 81–107.

Harley, S. & Kelly, N. 2007. The impact of zircon–garnet REE distribution data on the interpretation of zircon U–Pb ages in complex high-grade terrains: An example from the Rauer Islands, East Antarctica. *Chemical Geology*, **241**, 62–87.

Harley, S.L., Kelly, N.M. & Möller, A. 2007. Zircon behaviour and the thermal histories of mountain chains. *Elements*, **3**, 25–30.

Harrison, T.M. & Watson, E.B. 1983. Kinetics of zircon dissolution and zirconium diffusion in granitic melts of variable water content. *Contributions to Mineralogy and Petrology*, **84**, 66–72.

Harrison, T.M., Watson, E.B. & Aikman, A.B. 2007. Temperature spectra of zircon crystallization in plutonic rocks. *Geology*, **35**, 635–638.

Hermann, J. & Rubatto, D. 2003. Relating zircon and monazite domains to garnet growth zones: Age and duration of granulite facies metamorphism in the Val Malenco lower crust. *Journal of Metamorphic Geology*, **21**, 833–852.

Holland, T.J.B. & Powell, R. 1998. An internally consistent thermodynamic data set for phases of petrological interest. *Journal of Metamorphic Geology*, **16**, 309–343.

Jeon, H., Williams, I.S. & Chappell, B.W. 2012. Magma to mud to magma: Rapid crustal recycling by Permian granite magmatism near the eastern Gondwana margin. *Earth and Planetary Science Letters*, **319**, 104–117.

Johnson, T.E., White, R.W. & Powell, R. 2008. Partial melting of metagreywacke: A calculated mineral equilibria study. *Journal of Metamorphic Geology*, **26**, 837–853.

Kelsey, D.E. & Powell, R. 2011. Progress in linking accessory mineral growth and breakdown to major mineral evolution in metamorphic rocks: A thermodynamic approach in the Na_2O–CaO–K_2O–FeO–MgO–Al_2O_3–SiO_2–H_2O–TiO_2–ZrO_2 system. *Journal of Metamorphic Geology*, **29**, 151–166.

Kelsey, D.E., Clark, C. & Hand, M. 2008. Thermobarometric modelling of zircon and monazite growth in melt-bearing systems: Examples using model metapelitic and metapsammitic granulites. *Journal of Metamorphic Geology*, **26**, 199–212.

Korhonen, F.J., Saito, S., Brown, M. & Siddoway, C.S. 2010*a*. Modeling multiple melt loss events in the evolution of an active continental margin. *Lithos*, **116**, 230–248.

Korhonen, F.J., Saito, S., Brown, M., Siddoway, C.S. & Day, J.M.D. 2010*b*. Multiple generations of granite in the Fosdick Mountains, Marie Byrd Land, West Antarctica: Implications for polyphase intracrustal differentiation in a continental margin setting. *Journal of Petrology*, **51**, 627–670.

Korhonen, F.J., Clark, C., Brown, M., Bhattacharya, S. & Taylor, R. 2013*a*. How long-lived is ultrahigh temperature (UHT) metamorphism? Constraints from zircon and monazite geochronology in the Eastern Ghats orogenic belt, India. *Precambrian Research*, **234**, 322–350.

Korhonen, F.J., Brown, M., Clark, C. & Bhattacharya, S. 2013*b*. Osumilite–melt interactions in ultrahigh temperature granulites: Phase equilibria modelling and implications for the *P–T–t* evolution of the Eastern Ghats Province, India. *Journal of Metamorphic Geology*, **31**, 881–907.

Moecher, D.P., Samson, S.D. & Miller, C.F. 2004. Precise time and conditions of peak Taconian granulite facies metamorphism in the Southern Appalachian Orogen, USA, with implications for zircon behavior during crustal melting events. *Journal of Geology*, **112**, 289–304.

Morfin, S., Sawyer, E.W. & Bandyayera, D. 2013. Large volumes of anatectic melt retained in granulite facies migmatites: An injection complex in northern Quebec. *Lithos*, **168–169**, 200–218.

Nemchin, A. & Bodorkos, S. 2000. Zr and LREE concentrations in anatectic melt as a function of crystal size distributions of zircon and monazite in the source region. *Geological Society of America, Abstracts and Programs*, Abstract 52286.

Nemchin, A.A., Giannini, L.M., Bodorkos, S. & Oliver, N.H.S. 2001. Ostwald ripening as a possible mechanism for zircon overgrowth formation during anatexis: Theoretical constraints, a numerical model, and its application to pelitic migmatites of the Tickalara Metamorphics, northwestern Australia. *Geochimica et Cosmochimica Acta*, **65**, 2771–2788.

O'Brien, P.J. & Rötzler, J. 2003. High-pressure granulites: Formation, recovery of peak conditions and implications for tectonics. *Journal of Metamorphic Geology*, **21**, 3–20.

Powell, R. & Holland, T.J.B. 1988. An internally consistent dataset with uncertainties and correlations. 3. Applications to geobarometry, worked examples and a computer-program. *Journal of Metamorphic Geology*, **6**, 173–204.

Rapp, R.P. & Watson, E.B. 1986. Monazite solubility and dissolution kinetics: Implications for the thorium and light rare earth chemistry of felsic magmas. *Contributions to Mineralogy and Petrology*, **94**, 304–316.

Rapp, R.P., Ryerson, F. & Miller, C.F. 1987. Experimental evidence bearing on the stability of monazite during crustal anaatexis. *Geophysical Research Letters*, **14**, 307–310.

Redler, C., White, R.W. & Johnson, T.E. 2013. Migmatites in the Ivrea Zone (NW Italy): Constraints on partial melting and melt loss in metasedimentary rocks from Val Strona di Omegna. *Lithos*, **175–176**, 40–53.

Reno, B.L., Piccoli, P.M., Brown, M. & Trouw, R.A.J. 2012. *In situ* monazite (U–Th)–Pb ages from the Southern Brasília Belt, Brazil: Constraints on the high-temperature retrograde evolution of HP granulites. *Journal of Metamorphic Geology*, **30**, 81–112.

Roberts, M.P. & Finger, F. 1997. Do U–Pb zircon ages from granulites reflect peak metamorphic conditions? *Geology*, **25**, 319–322.

Rosenberg, C.L. & Handy, M.R. 2005. Experimental deformation of partially melted granite revisited: Implications for the continental crust. *Journal of Metamorphic Geology*, **23**, 19–28.

Rubatto, D. 2002. Zircon trace element geochemistry: Partitioning with garnet and the link between U–Pb ages and metamorphism. *Chemical Geology*, **184**, 123–138.

Rubatto, D., Williams, I.S. & Buick, I.S. 2001. Zircon and monazite response to prograde metamorphism in the Reynolds Range, central Australia. *Contributions to Mineralogy and Petrology*, **140**, 458–468.

Rubatto, D., Hermann, J. & Buick, I.S. 2006. Temperature and bulk composition control on the growth of monazite and zircon during low-pressure anatexis (Mount Stafford, central Australia). *Journal of Petrology*, **47**, 1973–1996.

Rubatto, D., Chakraborty, S. & Dasgupta, S. 2013. Timescales of crustal melting in the Higher Himalayan Crystallines (Sikkim, Eastern Himalaya) inferred from trace element-constrained monazite and zircon chronology. *Contributions to Mineralogy and Petrology*, **165**, 349–372.

Rudnick, R.L. & Gao, S. 2003. Composition of the continental crust. *In:* Rudnick, R.L. (ed.) *The Crust*. Treatise on Geochemistry, Elsevier, Amsterdam, **3**, 1–64.

Sandiford, M. & McLaren, S. 2002. Tectonic feedback and the ordering of heat producing elements within the continental lithosphere. *Earth and Planetary Science Letters*, **204**, 133–150.

Sandiford, M., McLaren, S. & Neumann, N. 2002. Long-term thermal consequences of the redistribution of heat-producing elements associated with large-scale granitic complexes. *Journal of Metamorphic Geology*, **20**, 87–98.

Sawyer, E. 1986. The influence of source rock type, chemical weathering and sorting on the geochemistry of clastic sediments from the Quetico metasedimentary belt, Superior Province, Canada. *Chemical Geology*, **55**, 77–95.

Sawyer, E. 1991. Disequilibrium melting and the rate of melt–residuum separation during migmatization of mafic rocks from the Grenville Front, Quebec. *Journal of Petrology*, **32**, 701–738.

Sawyer, E.W. & Barnes, S.J. 1988. Temporal and compositional differences between subsolidus and anatectic migmatite leucosomes from the Quetico metasedimentary belt, Canada. *Journal of Metamorphic Geology*, **6**, 437–450.

Skrzypek, E., Štípská, P. & Cocherie, A. 2012. The origin of zircon and the significance of U–Pb ages in high-grade metamorphic rocks: A case study from the Variscan orogenic root (Vosges Mountains, NE France). *Contributions to Mineralogy and Petrology*, **164**, 935–957.

Solar, G.S. & Brown, M. 2001. Petrogenesis of migmatites in Maine, USA: possible source of peraluminous leucogranite in plutons? *Journal of Petrology*, **42**, 789–823.

Spear, F.S. & Pyle, J.M. 2010. Theoretical modeling of monazite growth in a low-Ca metapelite. *Chemical Geology*, **273**, 111–119.

Stepanov, A.S., Hermann, J., Rubatto, D. & Rapp, R.P. 2012. Experimental study of monazite/melt partitioning with implications for the REE, Th and U geochemistry of crustal rocks. *Chemical Geology*, **300**, 200–220.

Taylor, S.R. & McLennan, S.M. 1985. *The continental crust: Its composition and evolution*. Blackwell Scientific, Oxford.

Teyssier, C. & Whitney, D.L. 2002. Gneiss domes and orogeny. *Geology*, **30**, 1139–1142.

Tomkins, H., Powell, R. & Ellis, D. 2007. The pressure dependence of the zirconium-in-rutile thermometer. *Journal of Metamorphic Geology*, **25**, 703–713.

Vavra, G., Gebauer, D., Schmid, R. & Compston, W. 1996. Multiple zircon growth and recrystallization during polyphase Late Carboniferous to Triassic metamorphism in granulites of the Ivrea Zone (Southern Alps): An ion microprobe (SHRIMP) study. *Contributions to Mineralogy and Petrology*, **122**, 337–358.

Villaseca, C., Martín Romera, C., De La Rosa, J. & Barbero, L. 2003. Residence and redistribution of REE, Y, Zr, Th and U during granulite-facies metamorphism: Behaviour of accessory and major phases in peraluminous granulites of central Spain. *Chemical Geology*, **200**, 293–323.

Villaseca, C., Orejana, D. & Paterson, B.A. 2007. Zr–LREE rich minerals in residual peraluminous granulites, another factor in the origin of low Zr–LREE granitic melts? *Lithos*, **96**, 375–386.

Watson, E.B. 1996. Dissolution, growth and survival of zircons during crustal fusion: Kinetic principals, geological models and implications for isotopic inheritance. *Transactions of the Royal Society of Edinburgh: Earth Sciences*, **87**, 43–56.

Watson, E.B. & Harrison, T.M. 1983. Zircon saturation revisited: Temperature and composition effects in a variety of crustal magma types. *Earth and Planetary Science Letters*, **64**, 295–304.

Watson, E.B., Vicenzi, E.P. & Rapp, R.P. 1989. Inclusion/host relations involving accessory minerals in high-grade metamorphic and anatectic rocks. *Contributions to Mineralogy and Petrology*, **101**, 220–231.

Watt, G. & Harley, S. 1993. Accessory phase controls on the geochemistry of crustal melts and restites produced during water-undersaturated partial melting. *Contributions to Mineralogy and Petrology*, **114**, 550–566.

Watt, G.R., Burns, I.M. & Graham, G.A. 1996. Chemical characteristics of migmatites: Accessory phase distribution and evidence for fast melt segregation rates. *Contributions to Mineralogy and Petrology*, **125**, 100–111.

White, R.W. & Powell, R. 2002. Melt loss and the preservation of granulite facies mineral assemblages. *Journal of Metamorphic Geology*, **20**, 621–632.

White, R.W., Powell, R. & Clarke, G.L. 2003. Prograde metamorphic assemblage evolution during partial melting of metasedimentary rocks at low pressures: migmatites from Mt Stafford, Central Australia. *Journal of Petrology*, **44**, 1937–1960.

White, R.W., Pomroy, N.E. & Powell, R. 2005. An *in situ* metatexite–diatexite transition in upper amphibolite facies rocks from Broken Hill, Australia. *Journal of Metamorphic Geology*, **23**, 579–602.

White, R.W., Powell, R. & Holland, T.J.B. 2007. Progress relating to calculation of partial melting equilibria for metapelites. *Journal of Metamorphic Geology*, **25**, 511–527.

Whitehouse, M.J. & Platt, J.P. 2003. Dating high-grade metamorphism—constraints from rare-earth elements in zircon and garnet. *Contributions to Mineralogy and Petrology*, **145**, 61–74.

Whitney, D.L., Teyssier, C., Rey, P. & Buck, W.R. 2013. Continental and oceanic core complexes. *Geological Society of America Bulletin*, **125**, 273–298.

Williams, I. 2001. Response of detrital zircon and monazite, and their U–Pb isotopic systems, to regional metamorphism and host-rock partial melting, Cooma Complex, southeastern Australia. *Australian Journal of Earth Sciences*, **48**, 557–580.

Williams, M.L., Jercinovic, M.J. & Hetherington, C.J. 2007. Microprobe monazite geochronology: understanding geologic processes by integrating composition and chronology. *Annual Review of Earth and Planetary Sciences*, **35**, 137–175.

Yakymchuk, C. & Brown, M. 2014. Consequences of open-system melting in tectonics. *Journal of the Geological Society, London*, **171**, 21–40.

Yakymchuk, C., Brown, M., Ivanic, T.J. & Korhonen, F.J. 2013. Effect of anisotropy on the spatial distribution of leucosome in stromatic metatexite migmatite. *Tectonophysics*, **603**, 136–154.

Zack, T., Moraes, R. & Kronz, A. 2004. Temperature dependence of Zr in rutile: Empirical calibration of a rutile thermometer. *Contributions to Mineralogy and Petrology*, **148**, 471–488.

Zeng, L., Asimow, P.D. & Saleeby, J.B. 2005*a*. Coupling of anatectic reactions and dissolution of accessory phases and the Sr and Nd isotope systematics of anatectic melts from a metasedimentary source. *Geochimica et Cosmochimica Acta*, **69**, 3671–3682.

Zeng, L., Saleeby, J.B. & Asimow, P. 2005*b*. Nd isotope disequilibrium during crustal anatexis: A record from the Goat Ranch migmatite complex, southern Sierra Nevada batholith, California. *Geology*, **33**, 53–56.

Zeng, L., Saleeby, J.B. & Ducea, M. 2005*c*. Geochemical characteristics of crustal anatexis during the formation of migmatite at the Southern Sierra Nevada, California. *Contributions to Mineralogy and Petrology*, **150**, 386–402.

Received 23 September 2013; revised typescript accepted 20 February 2014.
Scientific editing by Chris Clark.